

Journal Pre-proof

A novel chalcone derivative as Nrf2 activator attenuates learning and memory impairment in a scopolamine-induced mouse model

Hyeon Jeong Kim, Bo Ko Jang, Jong-Hyun Park, Ji Won Choi, Sun Jun Park, Seong Rim Byeon, Ae Nim Pae, Yong Sup Lee, Eunji Cheong, Ki Duk Park



PII: S0223-5234(19)30929-8

DOI: <https://doi.org/10.1016/j.ejmech.2019.111777>

Reference: EJMECH 111777

To appear in: *European Journal of Medicinal Chemistry*

Received Date: 16 July 2019

Revised Date: 1 October 2019

Accepted Date: 9 October 2019

Please cite this article as: H.J. Kim, B.K. Jang, J.-H. Park, J.W. Choi, S.J. Park, S.R. Byeon, A.N. Pae, Y.S. Lee, E. Cheong, K.D. Park, A novel chalcone derivative as Nrf2 activator attenuates learning and memory impairment in a scopolamine-induced mouse model, *European Journal of Medicinal Chemistry* (2019), doi: <https://doi.org/10.1016/j.ejmech.2019.111777>.

This is a PDF file of an article that has undergone enhancements after acceptance, such as the addition of a cover page and metadata, and formatting for readability, but it is not yet the definitive version of record. This version will undergo additional copyediting, typesetting and review before it is published in its final form, but we are providing this version to give early visibility of the article. Please note that, during the production process, errors may be discovered which could affect the content, and all legal disclaimers that apply to the journal pertain.

© 2019 Published by Elsevier Masson SAS.

A Novel Chalcone Derivative as Nrf2 Activator Attenuates Learning and Memory Impairment in a Scopolamine-Induced Mouse Model

Hyeon Jeong Kim^{a,b,1}, Bo Ko Jang^{a,1}, Jong-Hyun Park^a, Ji Won Choi^a, Sun Jun Park^{a,c}, Seong Rim Byeon^d, Ae Nim Pae^{a,c,e}, Yong Sup Lee^{e,f}, Eunji Cheong^b, and Ki Duk Park^{a,c,e,*}

^aConvergence Research Center for Diagnosis, Treatment and Care System of Dementia, Korea Institute of Science and Technology (KIST), Seoul 02792, Republic of Korea

^bDepartment of Biotechnology, Yonsei University, Seoul 03722, Republic of Korea

^cDivision of Bio-Medical Science & Technology, KIST School, Korea University of Science and Technology, Seoul 02792, Republic of Korea

^dKainos Medicine, Inc. Daewangpangyo-ro, Seongnam, Gyeonggi 13488, Republic of Korea

^eKHU-KIST Department of Converging Science and Technology, Kyung Hee University, Seoul 02447, Republic of Korea

^fDepartment of Life and Nanopharmaceutical Sciences, College of Pharmacy, Kyung Hee University, Seoul 02447, Republic of Korea

¹ These authors contributed equally to this article.

* Corresponding author

Ki Duk Park, PhD; Convergence Research Center for Diagnosis, Treatment and Care System of Dementia, Korea Institute of Science and Technology, 39-1 Hawolgok-dong, Seongbuk-gu, Seoul, Republic of Korea. TEL: 82-2-958-5132, Fax: +82-2-958-5189, E-mail: kdpark@kist.re.kr

Abstract

Alzheimer's disease is a common neurodegenerative disease characterized by progressive degeneration and neuronal cell death, resulting in neural network dysfunction. As the underlying mechanisms, oxidative damage and neuroinflammation have been reported to contribute to the onset and deterioration of Alzheimer's disease. The nuclear factor E2-related factor 2-antioxidant responsive element (Nrf2-ARE) signaling pathway is a pivotal cellular defense mechanism against oxidative stress. Nrf2, a transcription factor, regulates the cellular redox balance and is primarily involved in anti-inflammatory responses. In this study, we synthesized novel chalcone derivatives and found a highly potent Nrf2 activator, compound **20a**. Compound **20a** confirmed to activate Nrf2 and induce expression of the Nrf2-dependent enzymes HO-1 and GCLC at both mRNA and protein levels. It also suppressed the production of nitric oxide and downregulated inflammatory mediators in BV-2 microglial cells. We found that compound **20a** effectively increased the expression level and the activity of superoxide dismutase (SOD) in both BV-2 microglial cells and brain hippocampus region of the scopolamine-induced mouse model. In addition, compound **20a** effectively recovered the learning and memory impairment in a scopolamine-induced mouse model.

Keywords

Alzheimer's disease; Nuclear factor erythroid 2-related factor 2; Chalcone; Oxidative stress; Superoxide dismutase

Highlights

A novel series of chalcone derivatives were synthesized as Nrf2 activators.

Compound **20a** increases antioxidant enzyme expression by nuclear translocation of Nrf2.

20a suppresses reactive oxygen species against oxidative stress in microglia.

20a increases expression level and activity of superoxide dismutase *in vitro* and *in vivo*.

20a restores scopolamine-induced memory impairment in mice.

1. Introduction

Alzheimer's disease (AD) is a progressive neurodegenerative disease with memory deficits and cognitive impairment. It is characterized by the accumulation of amyloid plaques and abnormally phosphorylated neurofibrillary tangles, mitochondrial abnormalities, and oxidative stress, which cause neural network dysfunction and death of neurons, especially in the cerebral cortex and hippocampus. [1, 2] In addition to these pathological hallmarks, many studies have proposed that oxidative stress and neuroinflammation can cause and accelerate AD. Chronic inflammatory processes are remarkably activated in the brains of AD patients. [3] Furthermore, the number of activated microglia that produce reactive oxygen species (ROS), nitric oxide (NO) and pro-inflammatory cytokines such as interleukin 6 (IL-6) and tumor necrosis factor- α (TNF- α) is increased [4, 5], indicating that antioxidant and anti-inflammatory therapeutic approaches can be beneficial in AD by suppressing neurotoxic responses.

The nuclear factor E2-related factor 2-antioxidant response element (Nrf2-ARE) signaling pathway is a primary cellular defense mechanism against oxidative damage. Under oxidative stressed conditions, the transcription factor Nrf2 regulates cellular redox balance through the induction of antioxidant enzyme genes such as heme oxygenase-1 (HO-1), NAD(P)H quinone oxidoreductase 1 (NQO1), and glutamate-cysteine ligase (GCL). [6, 7] Nrf2 has also been shown to contribute to the anti-inflammatory process. It has been reported that activation of Nrf2 suppresses the expression of cell adhesion molecules such as E-selectin and vascular cell adhesion molecule 1 (VCAM-1) [8, 9], as well as the induction of pro-inflammatory cytokines and enzymes, including cyclooxygenase-2 (COX-2) and inducible nitric oxide synthase (iNOS). [10-13] The Nrf2 signaling inhibits ROS-associated nuclear factor (NF)- κ B activation by inducing the antioxidant responses and blocking the

degradation of inhibitor of κB α ($\text{I}\kappa\text{B}\alpha$). [14-16] In addition, recent studies suggested that activation of Nrf2 inhibits NLRP3 inflammasome assembly and activation. [17, 18] These results demonstrate that Nrf2 plays a crucial role in anti-inflammatory responses as well as antioxidant defenses.

Based on this cytoprotective role of Nrf2, its signaling pathway is believed to be involved in protection against various neurodegenerative diseases, including AD, Parkinson's disease (PD), and multiple sclerosis (MS). [19, 20] Nrf2-deficient mice exhibit enhanced sensitivity to a variety of chemical and biological stresses and neurotoxicants and they are highly susceptible to inflammatory diseases. [7, 14] Nuclear Nrf2 and its target genes are also downregulated in the brains of AD patients [21] and mouse models of AD. [22, 23] Conversely, overexpression of Nrf2 suppressed the pathology of AD with memory improvement in a mouse model of AD. [24] Thus, Nrf2 activation is an attractive therapeutic target for AD through anti-inflammatory and antioxidant effects.

Small molecules that activate Nrf2 signaling have been investigated for the development of potential anti-inflammatory agents, but dimethyl fumarate (DMF, brand name TecfideraTM), developed to treat patients with relapsing-remitting multiple sclerosis (RRMS), is the only drug approved by the FDA. Chalcone, which contains a unique α,β -unsaturated ketone, is a representative compound that activates Nrf2 and has been reported to expand to many disease drugs including anti-inflammatory, anti-cancer, neuroprotective and beta-amyloid disaggregate agents (Figure 1). [25-32] In particular, novel chalcone derivatives have recently been reported for AD-related targets. [33, 34] In the present study, we synthesized a novel series of chalcone derivatives as Nrf2 activators and evaluated their Nrf2-activating efficacies, discovering an excellent Nrf2 activating compound (**20a**) (Figure 1). Compound **20a** was further evaluated for its antioxidant and anti-inflammatory effects in activated

microglia. We also investigated whether Nrf2 activation by compound **20a** could restore the memory deficits using a scopolamine-induced amnesia mouse model, an acute model with oxidative stress, neuroinflammation and cognitive impairment. [35-39]

Journal Pre-proof

2. Results

2.1. Compound 20a is a new and potent Nrf2 activator

Kumar et al reported that novel chalcone derivatives effectively activated Nrf2 through Keap1 modification and the most potent derivative (**21**, Table S1 in the Supporting Information) was further evaluated for its ability to induce Nrf2-dependent antioxidant genes. [26] In our previous study, [40] we optimized vinyl sulfones by introducing nitrogen heterocycles to improve the Nrf2 activating efficacy and druglike properties. In the present study, in order to optimize chalcone scaffold as Nrf2 activators, we synthesized chalcone derivatives containing heterocyclic amines such as morpholine, pyrrolidine and *N*-methylpiperazine (Scheme 1 and 2). To evaluate the Nrf2-activating ability of the synthesized compounds, we assessed their ability to release Nrf2 from Kelch-like ECH-associated protein 1 (Keap1) and translocate Nrf2 into the nucleus using our previously reported cell-based assay system. [40, 41] The potency of Nrf2 activation is shown in Table 1 as half maximal effective concentration (EC₅₀) values. Most derivatives (**5**, **6a-e**, **6g**, **9**, **11**, **14**, **17**, **20**) significantly activated Nrf2 nuclear translocation compared to that of DMF (EC₅₀: **5**, **6a-e**, **6g**, **9**, **11**, **14**, **17**, **20** = 0.63–3.33 μM vs DMF = 5.11 μM). First, we introduced a propylmorpholine group into the 2-, 3-, and 4-OH of ring A (**4-6**). In these three series of compounds, substitution the 4-position substituted derivatives (**6**) showed more potent Nrf2 translocation effects than the corresponding 2- and 3-position derivatives (**4**, **5**) (**6a** = 1.36 μM > **5a** = 2.30 μM & **6d** = 1.63 μM > **5b** = 1.72 μM > **4** = 5.52 μM). We also found that 2'-position substituted derivatives (**6a**: 2'-CF₃, EC₅₀ = 1.36 μM; **6d**: 2'-OMe, EC₅₀ = 1.63 μM) exhibited better activities than the corresponding 3'- and 4'-position substituted derivatives (**6b**: 3'-CF₃, EC₅₀ = 2.06 μM; **6e**: 3'-OMe, EC₅₀ = 2.58 μM; **6c**: 4'-CF₃, EC₅₀ = 2.43 μM; **6f**: 4'-OMe, EC₅₀ = 6.97 μM). In addition, the replacement of propylmorpholine at 4-hydroxyl

group of ring A with propylpyrrolidine slightly enhanced the Nrf2 activation effect (**9b**: $EC_{50} = 0.99 \mu\text{M}$ vs **6d**: $EC_{50} = 1.63 \mu\text{M}$). Next, we synthesized derivatives (**14**, **17**, **20**) that weakened the basicity of heterocyclic amines, including ketone group, based on previously the most active compound **6a**. All synthesized derivatives exerted significant Nrf2 activation effects ($EC_{50} = 0.63 \mu\text{M}$ – $1.91 \mu\text{M}$). Among them, compound **20a** has the highest Nrf2 activating potency and is superior to the well-known strong Nrf2 activator, sulforaphane (SFN) (EC_{50} : **20a** = $0.63 \mu\text{M}$ vs SFN = $0.88 \mu\text{M}$). In our previous study, [42] we analyzed the expression level of HO-1, a major Nrf2-dependent gene, using a sandwich enzyme-linked immunosorbent assay (ELISA) to compare Nrf2 activating efficacy among the synthesized compounds. To confirm the Nrf2 activating efficacy of the present class, we performed an ELISA assay for positive controls and the selected nine compounds. We observed that the Nrf2 activation effect confirmed by ELISA analysis tended to be the same as in the Keap1-Nrf2 functional assay (Table S1 in the Supporting Information).

In addition, we examined in vitro ADME/Tox properties such as CYP inhibition, metabolic stabilities and blood-brain barrier (BBB) permeability. The selected compound **20a** showed low inhibitory effect on 5 major CYP isotypes and favorable metabolic stabilities (Table S2 in the Supporting Information). We also performed a parallel artificial membrane permeability assay-BBB test using a commercial kit and found that the permeability of **20a** might be favorable for CNS drugs (Table S2 in the Supporting Information). Subsequent experiments were performed to investigate whether the most potent compound could exhibit both antioxidant and anti-inflammatory properties through Nrf2 activation in BV-2 microglial cells.

2.2. Compound 20a induces Nrf2 nuclear translocation

The most potent compound **20a** showed concentration-dependent activation of Nrf2 nuclear translocation with an EC₅₀ of 0.634 μ M in the Keap1-Nrf2 nuclear translocation assay (Figure 2A). To further investigate the *in vitro* efficacies of compound **20a**, we first evaluated its cytotoxic effect on BV-2 microglial cells. It was confirmed that compound **20a** did not affect cell viability up to 10 μ M (Figure 2B). Next, to identify whether compound **20a** induces nuclear translocation of Nrf2 in BV-2 microglial cells, we measured the expression level of Nrf2 in the nucleus after treatment with compound **20a** in a time-dependent manner. The nuclear Nrf2 level increased to maximum at ~2 h when compound **20a** was treated at 10 μ M in BV-2 microglial cells (Figure 2C). We also measured Nrf2 levels in nuclear fraction and whole cell lysate after 6 h exposure to various concentrations of compound **20a**. Western blot data indicated that compound **20a** concentration-dependently increased the amount of nuclear Nrf2, with a significant increase at 0.1 μ M (Figure 2C). Because activated Nrf2 is released from Keap1 and is no longer subject to proteosomal degradation, the total Nrf2 level, as well as nuclear Nrf2, are expected to increase. Indeed, total cellular Nrf2 accumulated following treatment with compound **20a** (Figure 2D). Taken together, we confirmed that compound **20a** effectively induced the Nrf2 release from Keap1 and Nrf2 nuclear-translocation in BV-2 microglial cells.

2.3. Compound 20a induces gene expression of antioxidant enzymes and attenuates inflammatory responses in activated microglia

In previous studies Nrf2 activators have been reported to induce expression of antioxidant genes and suppress inflammatory responses as well as antioxidant defenses. [40-

42] Therefore, we evaluated whether Nrf2 activation with compound **20a** could have these beneficial effects. After nuclear translocation, the transcription factor Nrf2 binds to its specific promoter sequences, AREs, and induces the expression of several cytoprotective genes, which are involved in glutathione synthesis, ROS scavenging, and detoxification of xenobiotics against oxidative stress. [6] To confirm whether these Nrf2-dependent enzyme genes are induced by compound **20a** because of Nrf2 activation in microglial cells, we measured the gene expression level of HO-1, which is the enzyme that converts heme to biliverdin, ferrous iron, and carbon monoxide, and glutamate-cysteine ligase regulatory subunit (GCLM), the regulatory subunit of GCL responsible for glutathione synthesis. Pretreatment with compound **20a** for 8 h significantly upregulated the relative mRNA expression levels of *Ho-1* and *Gclm* in BV-2 microglial cells (Figure 3A, B). We also measured the protein levels of HO-1 and GCLM in a time-dependent manner after treatment with compound **20a**. At a concentration of 3 μ M, compound **20a** significantly increased the expression levels of HO-1 and GCLM with a maximum increase at ~6 h (Figure 3C–E). Next, western blot analysis revealed that both HO-1 and GCLM were concentration-dependently increased after 12 h exposure to various concentrations of compound **20a**, with >7-fold and >15-fold upregulation observed at 10 μ M, respectively. (Figure 3F–H). These results indicate that compound **20a** significantly induces the Nrf2-dependent gene expression by activating Nrf2 in BV-2 microglial cells.

The Nrf2 signaling pathway have been reported to contributes to the anti-inflammatory process by suppressing inflammatory mediators including NO, pro-inflammatory cytokines, and inflammatory enzymes such as COX-2 and iNOS. [13] It also has been suggested that the Nrf2 down-regulates inflammatory responses through increasing expression of HO-1, the major Nrf2-dependent antioxidant enzyme, and neutralizing ROS in

several studies using cell cultures and Nrf2 knockout mouse model. [43- 45] We further investigated whether compound **20a** can reduce lipopolysaccharide (LPS)-induced inflammatory responses in BV-2 microglial cells. LPS stimulation significantly increased NO production compared to that of the untreated control and this aberrant NO production was concentration-dependently reduced by compound **20a** (Figure 4A). To determine whether compound **20a** regulates the expression of iNOS resulting in inhibition of NO production, we measured protein expression levels of iNOS, an NO-synthesizing enzyme, after pretreatment of the LPS-stimulated BV-2 microglial cells with compound **20a** for 3 h. Western blot analysis revealed that up-regulated gene expression of iNOS due to LPS stimulation was also concentration-dependently inhibited by compound **20a**, with almost complete inhibition at 10 μ M compared to the levels in the LPS-untreated control (Figure 4B). Next, we assessed the anti-inflammatory effects of compound **20a** on the production of proinflammatory cytokines. LPS stimulation markedly increased the secretion of TNF- α and IL-6 in BV-2 microglial cells, whereas preincubation of the cells with compound **20a** for 3 h significantly suppressed the levels of both proinflammatory cytokines in a concentration-dependent manner (Figure 4C, D). Taken together, these results indicate that compound **20a** effectively down-regulates LPS-induced inflammation in microglia by suppressing inflammatory mediators, such as iNOS, TNF- α , and IL-6.

2.4. Compound 20a reduces ROS production in microglia

ROS, one of the main indicators of oxidative stress, are known to contribute to neurodegeneration by causing inflammation and neurotoxicity when overproduced. [46] To examine whether compound **20a** can effectively reduce ROS in oxidative condition, we

measured the amount of ROS produced after hydrogen peroxide (H_2O_2) treatment in cells pretreated with or without compound **20a**, using 2', 7'-Dichlorodihydrofluorescein diacetate (DCFH-DA), a fluorescent probe for intracellular ROS. Treatment with H_2O_2 significantly increased intracellular ROS production compared to that of the untreated control (Figure 5A). In contrast, pretreatment with compound **20a** for 24 h concentration-dependently inhibited this ROS production in microglial cells (Figure 5A). Furthermore, pretreatment with 10 μ M compound **20a** also suppressed the increase in ROS production induced by H_2O_2 treatment at all concentrations (Figure 5B). In addition, we detected intracellular ROS accumulation in BV-2 microglial cells through fluorescence imaging, which confirmed that excessive ROS accumulation due to H_2O_2 treatment was dramatically reduced by pretreatment with compound **20a** in a similar concentration-dependent manner (Figure 5C). These results show that compound **20a** suppresses ROS accumulation in microglial cells through its potent antioxidant activity.

2.5. Compound 20a increases expression and activity of SOD *in vitro* and *in vivo*

Superoxide dismutase (SOD) is an important Nrf2-dependent antioxidant enzyme that catalyzes the dismutation of superoxide radicals into H_2O_2 . The expression level and activity of SOD have been reported to be reduced in the brain and plasma of mild cognitive impairment and AD patients. [47-51] It indicates that oxidative stress occurs from the early stage of disease and compromised antioxidant defense system contribute to the progression and pathology of AD. To investigate whether compound **20a** upregulate the gene expression of SOD1, one of three human SODs located in the cytoplasm, we measured the protein levels of SOD1 after treatment with compound **20a** for 12 h. Similar to that of other Nrf2-regulated

enzymes (Figure 3F), the expression of SOD1 increased in a concentration-dependent manner (Figure 6A). We next examined the effect of compound **20a** on SOD activity. The activity of SOD in BV-2 microglial cells after treating with compound **20a** for 24 h increased in a concentration-dependent manner, which indicates that compound **20a** effectively upregulates the gene expression as well as the activity of this antioxidant enzyme (Figure 6B). We also examined the antioxidant effect of compound **20a** in H₂O₂-treated BV-2 microglial cells. We found that SOD activity was reduced to approximately 50% after 18 h exposure to 400 μM H₂O₂ in the microglia (Figure 6C). Pretreatment with compound **20a** remarkably restored the reduced SOD activity to a higher level than that of the H₂O₂-untreated control (Figure 6C). In addition, we determined whether compound **20a** could increase *in vivo* SOD activity in the brain hippocampus using the scopolamine-induced amnesia model (Figure 6D). Scopolamine, a nonselective muscarinic acetylcholine receptor antagonist, has been known to cause memory impairment by blocking central cholinergic signaling. [37-39] Furthermore, recent studies have reported that the scopolamine-induced amnesia model is accompanied by oxidative stress [38, 52], neuroinflammation [35, 36], upregulation of several AD-associated genes [53], and accumulation of amyloid β and phosphorylated tau proteins [52, 54], all of which are major pathological features of AD. The activity of SOD was reduced in the scopolamine-treated mice (2 mg/kg, *i.p.* injection) but was significantly restored to normal levels by pretreatment with compound **20a** (30 mg/kg/day, *p.o.* for 5 days) (Figure 6E). These results mean that compound **20a** actually afforded antioxidant effects against oxidative stress by enhancing expression and activity of SOD *in vitro* and *in vivo*.

2.6. Compound 20a restores learning and memory *in vivo*

To examine if Nrf2 activation with compound **20a** could lead to *in vivo* therapeutic efficacy in cognitive disorders, we performed behavioral tests using the scopolamine-induced amnesia model. We assessed spatial working memory using the Y-maze spontaneous alternation test. We treated mice with compound **20a** (30 mg/kg/day, *p.o.*) for 5 days and injected scopolamine (2 mg/kg, *i.p.* injection) before the test on the last day (Figure 7A). The scopolamine-treated mice showed a reduced percentage of spontaneous alternations compared to that of the vehicle-treated control mice (Figure 7B). However, treatment with compound **20a** remarkably recovered the reduced alternation percentage (Figure 7B). There was no difference in the total number of arm entries among the experimental groups, confirming that the changes in percent alternation were not caused by hyperactivity of the mice (Figure 7B). Next, we treated mice with compound **20a** (30 mg/kg/day, *p.o.*) for 5 days and learning and memory performance was examined using the passive avoidance test in the scopolamine-induced mouse model (1 mg/kg, *i.p.* injection on day 4) (Figure 7C). As shown in Figure 7D, the scopolamine-treated mice showed markedly shorter step-through latency than the vehicle-treated control mice did, indicating memory deficits induced by scopolamine. In contrast, the mice treated with compound **20a** showed improved latency to more than 70% of the vehicle-treated control level (Figure 7D). These results indicate that compound **20a** effectively restores learning and memory in the scopolamine-induced amnesia model, suggesting a potential therapeutic effect in AD.

3. Discussion and Conclusion

Oxidative stress and neuroinflammation have been proposed as major contributors or driving forces to the pathogenesis and progression of AD. [1, 3] There is no currently available disease-modifying treatment that consistently maintains cognitive function by suppressing the progression of neurodegeneration in AD. Thus, inducing antioxidant and anti-inflammatory effects via Nrf2 activation can be an attractive therapeutic strategy in AD. In this study, we presented a novel synthetic compound **20a** with highly potent efficacy to activate Nrf2. Compound **20a** showed antioxidant and anti-inflammatory effects *in vitro* and effectively ameliorated learning and memory impairment in the scopolamine-induced mouse model.

Keap1, a negative regulator of Nrf2, normally sequesters Nrf2 in the cytoplasm and causes its continuous degradation through the ubiquitin-proteasome pathway. Under oxidative stressed conditions, oxidants and electrophiles chemically modify several critical cysteine residues within Keap1, causing a conformational change and inactivation of the protein. As a result, Nrf2 is released from Keap1, translocates into the nucleus, and induces the expression of several cytoprotective genes. [6, 7] Through initial screening against nuclear translocation activity of Nrf2 (Table 1), we found that compound **20a** has potent Nrf2-activating efficacy. Compound **20a** also contains a unique chalcone structure, an α,β -unsaturated ketone, that is highly reactive with cellular nucleophiles such as the thiol group of cysteine. Several studies have shown that chalcone derivatives are potent activators of the Nrf2-ARE signaling pathway. [26, 55] We also previously reported that the α,β -unsaturated sulfone group activate Nrf2 via the Nrf2-Keap1 signaling pathway. [42] Accordingly, compound **20a** appears to induce nuclear translocation of Nrf2 due to the reactivity of the cysteine thiol group in Keap1.

Although the mechanism underlying Nrf2-dependent anti-inflammation is still not clear, previous studies have reported that Nrf2 essentially contributes to anti-inflammatory responses through crosstalk between Nrf2 and NF- κ B pathways or elimination of ROS by Nrf2-dependent antioxidant enzymes. [13] A recent study also revealed a novel mechanism by which Nrf2 directly suppresses the induction of proinflammatory cytokine transcription by binding to the promoter regions of proinflammatory cytokine genes. [12] The anti-inflammatory properties of compound **20a** are believed to be due to Nrf2 activation. Compound **20a** does not directly scavenge free radicals (data not shown). Therefore, Nrf2 activation in microglia by compound **20a** induces the expression of Nrf2-dependent antioxidant enzymes and the elimination of ROS, resulting in inhibition of the LPS-induced inflammatory responses.

We have also demonstrated *in vivo* therapeutic effects of compound **20a** in terms of cognitive deficit-related behaviors. Compound **20a** effectively restored SOD activity and memory performance in the scopolamine-induced amnesia model. Previous *in vivo* studies have shown that the Nrf2 signaling pathway has protective effects by modulating oxidative stress in various neurodegenerative diseases, including AD. [19, 21] The scopolamine-induced amnesia model is accompanied by oxidative stress, resulting in memory impairment, which is ameliorated by suppression of free radicals and lipid peroxidation. [38, 52] Recent studies have reported the neuroprotective effects of natural compounds or their metabolites extracted from leaves and food on scopolamine-induced memory deficits. [35, 36, 39, 56, 57] However, the molecular modes of action in which an Nrf2 activator directly affords protective effects against the scopolamine-induced model have rarely been evaluated. Our study suggests that Nrf2 activators represent potential therapeutic strategies for cognitive impairment recovery in the scopolamine-induced mouse model.

Journal Pre-proof

4. Materials and Methods

4.1. General method

The synthetic scheme for final compounds is described in Scheme 2 and Scheme 3. The reaction was monitored using analytical thin-layer chromatography (TLC) plates (Merck, Cat# 1.05715) at 254 nm UV light. The reactants were purified by silica gel column chromatography (Merck, Cat# 1.09385). Melting points were determined using an OptiMelt melting point equipment (Stanford Research System, Inc.). NMR (Nuclear magnetic resonance) spectra were obtained using Bruker spectrometers at 400 MHz / 300 MHz (¹H) or 100 MHz / 75 MHz (¹³C). High-resolution mass spectrometry (HRMS) data was obtained using electron scatter ionization (ESI) on a LTQ Orbitrap (Thermo Electron Corporation) instrument. All chemicals, solvents and reagents were purchased from commercial reagent sources as reagent grade without further purification.

4.1.1. General procedure for the compounds (Method A)

To an ethanol (EtOH) solution of the **3**, **8**, **10**, **13**, **16** and **18** (1.0 equiv) was added either lithium hydroxide (LiOH) (1.0 ~ 1.5 equiv) or lithium hydroxide monohydrate (1.0 ~ 1.5 equiv). The reaction mixture was stirred at room temperature (15 min) and then treated with the desired benzaldehyde (1.5 ~ 3.0 equiv). The reaction mixture was stirred at room temperature (2 h) and diluted with EtOAc (~150 mL) and washed with H₂O (3 × ~150 mL). The organic layer was dried with anhydrous Na₂SO₄ and concentrated in vacuo. The resulting residue was purified using column chromatography on SiO₂ to afford free form products. The salt form compounds (**4**, **5**, **6**, **9**, **11**, **20**) were prepared by addition of 4.0 M HCl to EtOAc solutions.

4.1.2. (E)-3-(2-Methoxyphenyl)-1-(2-(3-morpholinopropoxy)phenyl)prop-2-en-1-one hydrochloride (4)

Using Method A, **3a** (0.85 g, 3.23 mmol), 2-methoxybenzaldehyde (0.44 g, 3.29 mmol), lithium hydroxide monohydrate (0.13 g, 3.23 mmol) and ethanol (15 mL, 0.25 M) gave **4b** as a pale gray solid (1.13 g, 84%). mp: 163.0–165.0 °C; ¹H NMR (400 MHz, DMSO-*d*₆) δ 12.16 (br s, N⁺H), 8.14–7.85 (m, 3 Ar H, 2 trans H), 7.45–7.41 (m, Ar H), 7.10–6.99 (m, 4 Ar H), 4.20, (t, *J* = 5.92 Hz, CH₂), 3.88–3.30 (m, OCH₃, 8 piperazine H), 2.82 (s, NCH₃), 2.25 (t, *J* = 7.48 Hz, CH₂); ¹³C NMR (100 MHz, DMSO-*d*₆) δ 187.4, 162.0, 158.1, 137.6, 132.0, 130.7, 130.6, 128.3, 123.0, 121.7, 120.6, 114.4, 111.7, 65.2, 55.6, 52.9, 49.5, 48.0, 41.9, 23.1.

4.1.3 (E)-1-(3-(3-Morpholinopropoxy)phenyl)-3-(2-(trifluoromethyl)phenyl)prop-2-en-1-one hydrochloride (5a)

Using Method A, **3b**, (0.60 g, 2.28 mmol), 2-trifluoromethylbenzaldehyde (0.36 mL, 2.73 mmol), lithium hydroxide (0.12 g, 2.73 mmol) and ethanol (10 mL, 0.25 M) gave **5a** as a white powder (0.08 g, 48%). mp: 130.5–132.5 °C; ¹H NMR (400 MHz, DMSO-*d*₆) δ 11.11 (br s, N⁺H), 8.37 (d, *J* = 7.8 Hz, Ar H), 8.06–7.96 (m, 2 trans H), 7.87–7.79 (m, 3 Ar H), 7.71–7.67 (m, 2 Ar H), 7.54 (t, *J* = 7.96 Hz, Ar H), 7.31–7.28 (m, Ar H), 4.20 (t, *J* = 5.84 Hz, CH₂), 3.99–3.80 (m, 4 piperazine H), 3.47 (d, *J* = 12.3 Hz, CH₂), 3.31–3.26 (m, 2 piperazine H), 3.13–3.06 (m, CH₂); ¹³C NMR (100 MHz, DMSO-*d*₆) δ 189.1, 159.1, 139.0, 138.4, 133.4, 133.2, 131.0, 130.6, 129.4, 128.0 (q, *J*_{C-F} = 29.5 Hz), 126.7, 126.3 (q, *J*_{C-F} = 5.4 Hz), 124.6 (q, *J*_{C-F} = 272.4 Hz), 122.0, 120.5, 114.4, 65.9, 63.6, 53.9, 51.5, 23.4.

4.1.4. (E)-3-(2-Methoxyphenyl)-1-(3-(3-morpholinopropoxy)phenyl)prop-2-en-1-one hydrochloride (5b)

Using Method A, **3b** (0.88 g, 3.34 mmol), 2-methoxybenzaldehyde (0.46 g, 3.41 mmol), lithium hydroxide monohydrate (0.14 g, 3.34 mmol) and ethanol (15 mL, 0.25 M) gave **5** as a pale yellow solid (1.25 g, 89%). mp: 141.0–143.0 °C; ¹H NMR (400 MHz, DMSO-*d*₆) δ 11.53 (br s, N⁺H), 8.06 (d, *J* = 15.8 Hz, trans H), 8.00 (dd, *J* = 1.4 Hz, 7.7 Hz, ArH), 7.86 (d, *J* = 15.8 Hz, trans H), 7.75 (d, *J* = 7.8 Hz, ArH), 7.59 (s, ArH), 7.52–7.43 (m, 2 ArH), 7.25 (dd, *J* = 2.2 Hz, 8.1 Hz, Ar H), 7.12 (d, *J* = 8.2 Hz, Ar H), 7.03 (t, *J* = 7.5 Hz, Ar H), 4.18 (t, *J* = 6.0 Hz, 2 H), 3.95 (d, *J* = 9.7 Hz, 2 H), 3.89 (s, 3 H), 3.86 (d, *J* = 11.4 Hz, 2 H), 3.45 (d, *J* = 12.0 Hz, 2 H), 3.33–3.24 (m, 2 H), 3.18–3.04 (m, 2 H), 2.29–2.22 (m, 2 H); ¹³C NMR (100 MHz, DMSO-*d*₆) δ 188.9, 158.3 (d, *J* = 30.4 Hz), 139.1, 138.5, 132.3, 129.9, 128.4, 122.8, 121.7, 121.1, 120.6, 119.4, 113.6, 111.7.

4.1.5 (E)-3-(2-Chlorophenyl)-1-(3-(3-morpholinopropoxy)phenyl)prop-2-en-1-one hydrochloride (5c)

Using Method A, **3b** (0.60 g, 2.28 mmol), 2-chlorobenzaldehyde (0.31 mL, 2.73 mmol), lithium hydroxide (0.12 g, 2.73 mmol) and ethanol (10 mL, 0.25 M) gave **5c** as a white powder (0.12 g, 72%). mp: 165.0–167.0 °C; ¹H NMR (400 MHz, DMSO-*d*₆) δ 11.19 (br s, N⁺H), 8.28–8.25 (m, Ar H), 8.08–7.98 (m, 2 trans H), 7.82 (d, *J* = 7.72 Hz, Ar H), 7.66–7.65 (m, Ar H), 7.60–7.45 (m, 4 Ar H), 7.30–7.27 (m, Ar H), 4.20 (t, *J* = 6.0 Hz, CH₂), 3.99–3.95 (m, 2 piperazine H), 3.87–3.81 (m, 2 piperazine H), 3.47 (d, *J* = 12.3 Hz, CH₂), 3.31–3.26 (m, 2 piperazine H), 3.14–3.05 (m, 2 piperazine H), 2.29–2.22 (m, CH₂); ¹³C NMR (100

MHz, DMSO- d_6) δ 189.2, 159.1, 139.2, 139.1, 134.9, 132.7, 132.5, 130.5, 130.4, 129.2, 128.2, 125.3, 121.9, 120.4, 114.4, 65.8, 63.6, 53.9, 51.5, 23.4.

4.1.6. (*E*)-1-(4-(3-Morpholinopropoxy)phenyl)-3-(2-(trifluoromethyl)phenyl)pro-2-pen-1-one hydrochloride (6a)

Using Method A, **3c** (17.4 g, 65.9 mmol), 2-trifluorobenzaldehyde (8.86 g, 67.2 mmol), lithium hydroxide monohydrate (2.76 g, 65.9 mmol) and ethanol (525 mL, 0.125 M) gave **6a** as a white solid (24 g, 87%). mp: 209.0–211.0 °C; ^1H NMR (400 MHz, DMSO- d_6) δ 11.54 (br s, N^+H), 8.39 (d, $J = 7.8$ Hz, ArH), 8.25 (d, $J = 8.8$ Hz, 2 ArH), 8.09 (d, $J = 15.3$ Hz, trans H), 7.98 (d, $J = 15.3$ Hz, trans H), 7.88 (d, $J = 7.8$ Hz, ArH), 7.83 (t, $J = 7.8$ Hz, ArH), 7.70 (t, $J = 7.4$ Hz, ArH), 7.16 (d, $J = 8.8$ Hz, 2 ArH), 4.26 (t, $J = 5.9$ Hz, 2 H), 4.00 (d, $J = 12.2$ Hz, 2 H), 3.91 (t, $J = 12.1$ Hz, 2 H), 3.50 (d, $J = 12.1$ Hz, 2 H), 3.33–3.28 (m, 2 H), 3.16–3.09 (m, 2 H), 2.30–2.29 (m, 2 H); ^{13}C NMR (100 MHz, DMSO- d_6); δ 187.0, 162.6, 137.1, 133.0, 132.9, 131.2, 130.3, 130.2, 128.8, 127.5 (q, $J = 29.4$ Hz), 126.1, 124.2 (q, $J = 272.4$ Hz), 114.6, 65.6, 63.2, 53.3, 51.1, 22.9.

4.1.7. (*E*)-1-(4-(3-Morpholinopropoxy)phenyl)-3-(3-(trifluoromethyl)phenyl)pro-2-pen-1-one hydrochloride (6b)

Using Method A, **3c** (0.42 g, 1.59 mmol), 3-trifluorobenzaldehyde (0.22 mL, 1.63 mmol), lithium hydroxide monohydrate (0.07 g, 1.59 mmol) and ethanol (5 mL, 0.25 M) gave **6b** as a white solid (0.22 g, 30%). mp: 193.0–194.0 °C; ^1H NMR (400 MHz, MeOD) δ 8.16 (d, $J = 8.9$ Hz, 2 ArH), 8.03 (t, $J = 7.8$ Hz, 2 ArH), 7.90 (d, $J = 15.7$ Hz, trans H), 7.80 (d, $J = 15.7$

Hz, 2 trans **H**), 7.73 (d, $J = 7.6$ Hz, Ar**H**), 7.65 (t, $J = 7.6$ Hz, Ar**H**), 7.11 (d, $J = 8.8$ Hz, 2 Ar**H**), 4.25 (t, $J = 5.7$ Hz, 2 **H**), 4.18–3.97 (br m, 2 **H**), 3.91–3.71 (m, 2 **H**), 3.65–3.45 (br m, 2 **H**), 3.29 (t, $J = 8.0$ Hz, 2 **H**), 3.28–3.14 (br m, 2 **H**), 2.34–2.29 (m, 2 **H**); ^{13}C NMR (100 MHz, DMSO- d_6) δ 187.3, 162.5, 141.4, 136.0, 132.8, 131.2, 130.5, 129.9, 129.8 (q, $J = 31.9$ Hz), 126.5, 125.1, 124.1 (q, $J = 270.9$ Hz), 124.0, 114.6, 65.6, 63.2, 53.4, 51.1, 22.9.

4.1.8. (E)-1-(4-(3-Morpholinopropoxy)phenyl)-3-(4-(trifluoromethyl)phenyl)pro-2-pen-1-one hydrochloride (6c)

Using Method A, **3c** (0.44 g, 1.67 mmol), 4-trifluorobenzaldehyde (0.23 mL, 1.70 mmol), lithium hydroxide monohydrate (0.07 g, 1.67 mmol) and ethanol (7 mL, 0.25 M) gave **6c** as a pale green solid (0.20 g, 29%). mp: 203.0–205.0 °C; ^1H NMR (400 MHz, MeOD) δ 8.14 (m, 2 Ar**H**), 7.89–7.95 (m, trans **H**, 2 Ar**H**), 7.72–7.81 (m, trans **H**, 2 Ar**H**), 7.09–7.11 (m, 2 Ar**H**), 4.24 (t, $J = 5.7$ Hz, 2 **H**), 4.09 (d, $J = 12.3$ Hz, 2 **H**), 3.81 (t, $J = 12.5$ Hz, 2 **H**), 3.58 (d, $J = 12.2$ Hz, 2 **H**), 3.41 (t, $J = 8.0$ Hz, 2 **H**), 3.21 (t, $J = 12.2$ Hz, 2 **H**), 2.35–2.28 (m, 2 **H**); ^{13}C NMR (100 MHz, DMSO- d_6) δ 187.2, 162.4, 141.1, 138.8, 131.1, 130.3, 130.0, 129.9 (d, $J = 31.7$ Hz), 129.3, 125.6, 124.7, 124.0 (q, $J = 270.4$ Hz), 114.5, 65.5, 63.1, 53.3, 51.0, 22.8.

4.1.9. (E)-3-(2-Methoxyphenyl)-1-(4-(3-morpholinopropoxy)phenyl)prop-2-en-1-one hydro chloride (6d)

Using Method A, **3c** (0.30 g, 1.14 mmol), 4-trifluorobenzaldehyde (0.12 mL, 1.17 mmol), lithium hydroxide monohydrate (0.05 g, 1.14 mmol) and ethanol (5 mL, 0.25 M) gave **6d** as a white solid (0.12 g, 28%). mp: 211.0–213.0 °C; ^1H NMR (400 MHz, DMSO- d_6) δ 11.75 (s, N^+H), 8.15 (d, $J = 8.8$ Hz, 2 Ar**H**), 7.97–8.05 (m, Ar**H**, trans **H**), 7.89 (d, $J = 15.7$ Hz, trans

H), 7.42–7.47 (m, Ar**H**), 7.01–7.12 (m, 4 Ar**H**), 4.21 (t, $J = 6.0$ Hz, 2 **H**), 3.87–3.98 (m, 7 **H**), 3.46 (d, $J = 12.2$ Hz, 2 **H**), 3.24–3.29 (m, 2 **H**), 3.05–3.13 (m, 2 **H**), 2.24–2.31 (m, 2 **H**); ^{13}C NMR (100 MHz, DMSO- d_6) δ 188.0, 162.6, 158.6, 138.2, 132.6, 131.3, 131.2, 128.9, 123.5, 122.2, 121.1, 115.0, 112.3, 65.9, 63.6, 56.2, 53.8, 51.4, 23.3.

4.1.10. (E)-3-(3-Methoxyphenyl)-1-(4-(3-morpholinopropoxy)phenyl)prop-2-en-1-one hydrochloride (6e)

Using Method A, **3c** (0.35 g, 1.33 mmol), 3-methoxybenzaldehyde (0.16 mL, 1.36 mmol), lithium hydroxide monohydrate (0.06 g, 1.33 mmol) and ethanol (5 mL, 0.25 M) gave **6e** as a white solid (0.43 g, 77%). mp: 212.0–214.0 °C; ^1H NMR (400 MHz, DMSO- d_6) δ 11.52 (br s, N^+H), 8.19 (d, $J = 8.9$ Hz, 2 Ar**H**), 7.95 (d, $J = 15.6$ Hz, trans **H**), 7.67 (d, $J = 15.6$ Hz, trans **H**), 7.47 (s, Ar**H**), 7.43 (d, $J = 7.7$ Hz, Ar**H**), 7.36 (t, $J = 7.9$ Hz, Ar**H**), 7.09 (d, $J = 8.9$ Hz, 2 Ar**H**), 7.01 (dd, $J = 2.1$ Hz, 7.9 Hz, Ar**H**), 4.20 (t, $J = 6.1$ Hz, 2 **H**), 3.95 (d, $J = 11.5$ Hz, 2 **H**), 3.88 (d, $J = 12.2$ Hz, 2 **H**), 3.82 (s, 3 **H**), 3.45 (d, $J = 12.2$ Hz, 2 **H**), 3.30–3.20 (m, 2 Ar**H**), 3.14–3.02 (m, 2 **H**), 2.29–2.22 (m, 2 **H**); ^{13}C NMR (100 MHz, DMSO- d_6) δ 187.4, 162.3, 159.7, 143.2, 136.2, 131.0, 130.6, 130.0, 122.3, 121.6, 116.5, 114.5, 113.4, 65.4, 63.1, 55.3, 53.3, 51.0, 22.9.

4.1.11. (E)-3-(4-Methoxyphenyl)-1-(4-(3-morpholinopropoxy)phenyl)prop-2-en-1-one hydrochloride (6f)

Using Method A, **3c** (0.37 g, 1.41 mmol), 4-methoxybenzaldehyde (0.17 mL, 1.43 mmol), lithium hydroxide monohydrate (0.06 g, 1.41 mmol) and ethanol (6 mL, 0.25 M) gave **6f** as a white solid (0.30 g, 52%). mp: 192.0–194.0 °C; ^1H NMR (400 MHz, DMSO- d_6) δ 11.53 (br s, N^+H), 8.15 (d, $J = 8.7$ Hz, 2 Ar**H**), 7.79–7.85 (m, trans **H**, 2 Ar**H**), 7.67 (d, $J = 15.5$ Hz, trans

H), 7.08 (d, $J = 8.8$ Hz, 2 Ar**H**), 7.01 (d, $J = 8.7$ Hz, 2 Ar**H**), 4.19 (t, $J = 6.1$ Hz, 2 **H**), 3.95 (d, $J = 11.5$ Hz, 2 **H**), 3.88 (d, $J = 12.1$ Hz, 2 **H**), 3.81 (s, 3 **H**), 3.44 (d, $J = 12.1$ Hz, 2 **H**), 3.32–3.20 (m, 2 **H**), 3.11–3.04 (m, 2 **H**), 2.29–2.22 (m, 2 **H**); ^{13}C NMR (100 MHz, DMSO- d_6) δ 187.2, 162.1, 161.2, 143.2, 130.9, 130.8, 130.7, 127.4, 119.5, 114.4, 114.3, 65.4, 63.1, 55.4, 53.3, 51.0, 22.9.

4.1.12. (*E*)-3-(2-Chlorophenyl)-1-(4-(3-morpholinopropoxy)phenyl)prop-2-en-1-one (**6g**)

Using method A, **3c** (0.60 g, 2.28 mmol) and 2-chlorobenzaldehyde (0.31 mL, 2.73 mmol), lithium hydroxide (0.12 g, 2.73 mmol) and ethanol (10 mL, 0.25 M) gave **5c** as a white powder (0.63 g, 72%); ^1H NMR (400 MHz, DMSO- d_6) δ 8.24–8.17 (m, 3 Ar **H**), 8.01 (s, 2 Ar **H**), 7.59–7.44 (m, Ar **H**, 2 trans **H**), 7.09 (d, $J = 8.64$ Hz, 2 Ar **H**), 4.14 (t, $J = 6.24$ Hz, **CH**₂), 3.59–3.57 (m, 4 piperazine **H**), 2.45–2.37 (m, **CH**₂, 4 piperazine **H**), 1.95–1.88 (m, **CH**₂); ^{13}C NMR (100 MHz, DMSO- d_6) δ 187.6, 163.4, 138.2, 134.7, 132.9, 132.3, 131.6, 130.5, 129.0, 128.1, 125.3, 115.0, 66.8, 66.7, 55.2, 53.8, 26.2.

4.1.13. (*E*)-1-(4-(3-Morpholinopropoxy)phenyl)-3-(pyridin-2-yl)prop-2-en-1-one hydrochloride (**6h**)

Using Method A, **3c** (0.30 g, 1.14 mmol) and 2-pyridinecarboxaldehyde (0.11 mL, 1.16 mmol) and lithium hydroxide (0.05 g, 1.14 mmol) gave **6g** as a yellow powder (0.10 g, 25%); mp: 243.0–245.0 °C; ^1H NMR (400 MHz, CDCl₃) δ 11.45 (br s, 1**H**), 8.80 (d, $J = 5.1$ Hz, Ar**H**), 8.46 (d, $J = 15.6$ Hz, trans **H**), 8.19–8.28 (m, 4 Ar**H**), 7.72–7.80 (m, trans **H**, Ar**H**), 7.13 (d, $J = 9.0$ Hz, 2 Ar**H**), 4.22 (t, $J = 6.04$ Hz, 2 **H**), 3.83–3.98 (m, 4 **H**), 3.45 (d, $J = 12.1$ Hz, 2 **H**), 3.23–3.28 (m, 2 **H**), 3.03–3.12 (m, 2 **H**), 2.23–2.30 (m, 2 **H**); ^{13}C NMR (100 MHz,

CDCl_3) δ 187.4, 163.2, 150.7, 146.9, 142.0, 138.1, 131.7, 130.5, 128.8, 126.4, 126.3, 115.2, 66.0, 63.6, 53.7, 51.5, 23.3.

4.1.14. (E)-1-(4-(3-Morpholinophoxy)phenyl)-3-(pyridin-3-yl)prop-2-en-1-one hydrochloride (6i)

Using Method A, **3c** (0.30 g, 1.14 mmol) and 2-pyridinecarboxaldehyde (0.11 mL, 1.16 mmol) and lithium hydroxide (0.05 g, 1.14 mmol) gave **6h** as an ivory powder (0.15 g, 37%); mp: 115.0–116.0 °C; ^1H NMR (400 MHz, CDCl_3) δ 11.59 (br s, 1 **H**), 9.40 (s, Ar**H**), 8.96 (d, $J = 8.3$ Hz, Ar**H**), 8.87 (d, $J = 4.9$ Hz, Ar**H**), 8.32 (d, $J = 15.8$ Hz, trans **H**), 8.23 (d, $J = 8.8$ Hz, 2 Ar**H**), 8.01–8.05 (m, Ar **H**), 7.81 (d, $J = 15.7$ Hz, trans **H**), 7.13 (d, $J = 8.9$ Hz, 2 Ar**H**), 7.23 (t, $J = 6.0$ Hz, 2 **H**), 3.85–3.97 (m, 5 **H**), 3.45 (d, $J = 12.2$ Hz, 2 **H**), 3.23–3.25 (m, 2 **H**), 3.04–3.11 (m, 2 **H**), 2.23–2.30 (m, 2 **H**); ^{13}C NMR (100 MHz, CDCl_3) δ 187.3, 163.2, 144.0, 143.7, 143.0, 137.3, 134.2, 131.8, 130.5, 127.4, 127.1, 115.1, 66.0, 63.6, 53.7, 51.5, 23.3.

4.1.15. (E)-1-(4-(3-(Pyrrolidin-1-yl)propoxy)phenyl)-3-(2-(trifluoromethyl)phenyl)prop-2-en-1-one hydrochloride (9a)

Using Method A, **8** (1.00 g, 4.04 mmol), 2-(trifluoromethyl)benzaldehyde (1.00 mL, 8.08 mmol) and lithium hydroxide (0.15 g, 6.06 mmol) gave **9a** as an ivory solid (0.75 g, 42%). mp: 164.0–166.0 °C; ^1H NMR (400 MHz, $\text{DMSO}-d_6$) δ 10.76 (br s, N^+H), 8.35 (d, $J = 7.8$ Hz, 1 Ar**H**), 8.22 (d, $J = 8.7$ Hz, 2 Ar**H**), 8.06 (d, $J = 15.3$ Hz, trans **H**), 7.96 (d, $J = 15.3$ Hz, trans **H**), 7.86–7.79 (m, 2 Ar**H**), 7.68 (t, $J = 7.6$ Hz, 1 Ar **H**), 7.13 (d, $J = 8.7$ Hz, 2 Ar **H**), 4.23 (t, $J = 5.9$ Hz, OCH_2), 3.56 (br s, 2 pyrrolidine **H**), 3.30 (t, $J = 8.04$ Hz, NCH_2), 3.01 (br s, 2 pyrrolidine **H**), 2.24–2.18 (m, $\text{CH}_2\text{CH}_2\text{CH}_2$), 2.01 (br s, 2 pyrrolidine **H**), 1.91 (br s, 2 pyrrolidine **H**); ^{13}C NMR (100 MHz, CDCl_3) δ 187.4, 163.0, 137.5, 133.4, 131.7, 131.3,

131.1, 130.8, 130.5, 129.2, 127.9 (q, $J_{C-F} = 29.3$ Hz), 126.7, 126.6, 124.7 (q, $J_{C-F} = 272.0$ Hz), 155.1, 65.9, 53.3, 51.5, 25.5, 23.2.

4.1.16. (E)-3-(2-Methoxyphenyl)-1-(4-(3-(pyrrolidin-1-yl)propoxy)phenyl)prop-2-en-1-one hydrochloride (9b)

Using Method A, **8** (0.42 g, 1.70 mmol), 2-methoxybenzaldehyde (0.24 g, 1.73 mmol), lithium hydroxide monohydrate (0.07 g, 1.70 mmol) and ethanol (15 mL, 0.25 M) gave **9** as a pale brown solid (0.33 g, 48%). mp: 158.0–160.0 °C; ^1H NMR (400 MHz, DMSO- d_6) δ 11.09 (br s, N^+H), 8.14 (d, $J = 8.6$ Hz, 2 ArH), 8.02 (d, $J = 15.8$ Hz, trans H), 7.97 (d, $J = 7.5$ Hz, ArH), 7.88 (d, $J = 15.7$ Hz, trans H), 7.44 (t, $J = 7.4$ Hz, 1H), 7.10 (t, $J = 8.1$ Hz, 3 ArH), 7.03 (t, $J = 7.5$ Hz, ArH), 4.20 (t, $J = 5.9$ Hz, 2H), 3.89 (s, OCH_3), 3.60–3.50 (m, 2 H), 3.27 (q, $J = 6.8$ Hz, 2 H), 3.09–2.98 (m, 2 H), 2.22–2.18 (m, 2 H), 1.99–1.93 (m, 2 H), 1.90–1.87 (m, 2 H); ^{13}C NMR (100 MHz, DMSO- d_6) δ 187.3, 161.9, 157.9, 137.5, 131.9, 130.6, 130.5, 128.2, 122.8, 121.5, 120.5, 114.3, 111.6, 65.1, 55.5, 52.6, 50.8, 24.9, 22.5.

4.1.17. (E)-3-(2-Chlorophenyl)-1-(4-(3-(pyrrolidin-1-yl)propoxy)phenyl)prop-2-en-1-one hydrochloride (9c)

Using Method A, **8** (1.00 g, 4.04 mmol), 2-(trifluoromethyl)benzaldehyde (1.00 mL, 8.08 mmol) and lithium hydroxide (0.15 g, 6.06 mmol) gave **9c** an ivory solid (0.73 g, 41%) as a Ivory solid. mp: 184.0–186.0 °C; ^1H NMR (400 MHz, DMSO- d_6) δ 10.59 (br s, N^+H), 8.25–8.20 (m, 3 Ar H), 8.03 (s, 2 Ar H), 7.60–7.58 (m, 1 Ar H), 7.52–7.45 (m, 2 Ar H), 7.12 (d, $J = 8.9$ Hz, 2 Ar H), 4.23 (t, $J = 6.0$ Hz, OCH_2), 3.56 (br s, 2 pyrrolidine H), 3.30 (t, $J = 7.4$ Hz, 2 NCH_2), 3.02 (br s, 2 pyrrolidine H), 2.24–2.17 (m, $\text{CH}_2\text{CH}_2\text{CH}_2$), 2.02 (br s, 2

pyrrolidine **H**), 1.90 (br s, 2 pyrrolidine **H**); ^{13}C NMR (100 MHz, CDCl_3) δ 187.6, 162.9, 138.2, 134.7, 132.8, 132.3, 131.6, 130.7, 130.4, 129.0, 128.1, 125.2, 115.0, 65.8, 53.3, 51.5, 25.5, 23.2.

4.1.18. (E)-3-(2-Methoxyphenyl)-1-(4-(3-(4-methylpiperazin-1-yl)propoxy)phenyl)prop-2-en-1-one dihydrochloride (11)

Using Method E, **10** (0.36 g, 1.30 mmol), 2-methoxybenzaldehyde (0.18 g, 1.33 mmol), lithium hydroxide monohydrate (0.05 g, 1.30 mmol) and ethanol (10 mL, 0.25 M) gave **11** as a pale yellow solid (0.55 g, 89%). mp: 232.0–234.0 °C; ^1H NMR (400 MHz, $\text{DMSO-}d_6$) δ 12.16 (br s, 2 N^+H), 8.13 (d, $J = 8.8$ Hz, 2 ArH), 8.01 (d, $J = 15.7$ Hz, trans **H**), 7.96 (d, $J = 7.7$ Hz, ArH), 7.87 (d, $J = 15.7$ Hz, trans **H**), 7.44–7.40 (m, ArH), 7.09 (dd, $J = 8.3$ Hz, 8.8 Hz, 3 ArH), 7.01 (t, $J = 7.5$ Hz, ArH), 4.20 (t, $J = 6.0$ Hz, 2H), 3.88 (s, OCH_3), 3.81 (br s, 2H), 3.77 (br s, 2H), 3.69–3.49 (m, 4H), 3.30 (br s, 2H), 2.82 (s, 3H), 2.26–2.23 (m, 2H); ^{13}C NMR (100 MHz, $\text{DMSO-}d_6$) δ 187.4, 162.0, 158.0, 137.6, 132.0, 130.7, 130.6, 128.3, 123.0, 121.7, 120.6, 114.4, 111.7, 65.2, 55.6, 52.9, 49.5, 48.0, 23.1.

4.1.19. (E)-N,N-Dimethyl-2-(4-(3-(2-(trifluoromethyl)phenyl)acryloyl)phenoxy)acetamide (14a)

Using Method A, **13** (0.20 g, 0.90 mmol) and 2-(trifluoromethyl)benzaldehyde (0.10 mL, 1.08 mmol) and LiOH (0.02 g, 1.08 mmol) gave **14a** as a light yellow solid (0.15 g, 45%). $R_f = 0.45$ (Only EtOAc); mp: 122.0–123.0 °C; ^1H NMR (400 MHz, CDCl_3) δ 8.01–8.06 (m, trans **H**), 7.92–7.96 (m, 2H), 7.74 (d, $J = 7.8$ Hz, ArH), 7.64 (d, $J = 7.7$ Hz, ArH), 7.53 (t, $J =$

7.5 Hz, ArH), 7.42 (t, $J = 7.6$ Hz, ArH), 7.34 (d, $J = 15.5$, trans H), 6.94–6.98 (m, 2ArH), 4.71 (s, OCH₃), 3.02 (s, NCH₃), 2.92 (s, NCH₃); ¹³C NMR (75 MHz, CDCl₃) δ 188.5, 167.1, 161.6, 139.5 (d, $J = 1.92$ Hz), 134.2, 132.1, 131.4, 131.0, 129.8, 129.2 (q, $J = 30.2$ Hz), 128.0, 126.4, 126.3 (q, $J = 5.58$ Hz), 124.0 (q, $J_{C-F} = 272.4$ Hz), 114.7, 67.2, 36.5, 35.7; HRMS (M + H)⁺ (ESI⁺) 378.1310 [M + H]⁺ (calcd for C₂₀H₁₈F₃NO₃H⁺ 378.1312).

4.1.20. (E)-2-(4-(3-(2-Methoxyphenyl)acryloyl)phenoxy)-N,N-dimethyl acetamide (14b)

Using Method A, **13** (0.50 g, 2.26 mmol) and 2-methoxybenzaldehyde (0.46 g, 3.39 mmol) and LiOH (0.09 g, 2.26 mmol) gave **14b** as a light yellow solid (0.57 g, 100%). $R_f = 0.34$ (EtOAc/*n*-hexane 5/1); mp: 118.0–119.0 °C; ¹H NMR (400 MHz, DMSO-*d*₆) δ 8.10 (d, $J = 8.8$ Hz, 2 ArH), 7.95–8.03 (m, ArH, trans H), 7.87 (d, $J = 15.7$ Hz, trans H), 7.42–7.47 (m, ArH), 7.12 (d, $J = 8.3$ Hz, ArH), 7.02–7.06 (m, 3 ArH), 4.94 (OCH₂), 3.90 (OCH₃), 2.91 (s, NCH₃), 2.86 (s, NCH₃); ¹³C NMR (100 MHz, CDCl₃) δ 189.3, 167.1, 161.6, 158.8, 139.7, 132.1, 131.6, 130.8, 129.2, 124.0, 122.7, 120.7, 114.5, 111.3, 67.2, 55.5, 36.5, 35.7; HRMS (M + H)⁺ (ESI⁺) 340.1542 [M + H]⁺ (calcd for C₂₀H₂₁N₂O₄H⁺ 340.1543).

4.1.21. (E)-N,N-Dimethyl-2-(4-(3-(pyridin-2-yl)acryloyl)phenoxy)acetamide (14c)

Using Method A, **13** (0.20 g, 0.90 mmol), 2-pyridinecarboxaldehyde (0.26 mL, 2.70 mmol) and LiOH·H₂O (0.05 g, 1.10 mmol) gave **14c** as a yellow solid (0.11 g, 39%). $R_f = 0.10$ (Only EtOAc); ¹H NMR (400 MHz, DMSO-*d*₆) δ 8.69 (s, ArH), 8.07–8.16 (m, trans H, 2 ArH), 7.91 (s, 2 ArH), 7.69 (d, $J = 15.4$ Hz, trans H), 7.44 (s, ArH), 7.07 (d, $J = 8.2$ Hz, 2 ArH), 6.94 (d, 3.2 Hz, ArH), 4.98 (s, OCH₂), 3.01 (s, NCH₃), 2.86 (s, NCH₃); ¹³C NMR (100 MHz,

DMSO-*d*₆) δ 188.1, 167.1, 162.9, 153.4, 150.5, 142.8, 137.6, 131.2, 130.9, 130.7, 125.7, 125.2, 125.1, 115.3, 66.2, 36.0, 35.4; HRMS (M + H)⁺ (ESI⁺) 311.1383 [M + H]⁺ (calcd for C₁₈H₁₈N₂O₃H⁺ 311.1390).

4.1.22. (*E*)-*N,N*-Dimethyl-2-(4-(3-(pyridin-3-yl)acryloyl)phenoxy)acetamide (**14d**)

Using Method A, **13** (0.20 g, 0.90 mmol), 3-pyridinecarboxaldehyde (0.25 mL, 2.70 mmol) and LiOH·H₂O (0.05 g, 1.10 mmol) gave **14d** as a white solid (0.13 g, 47%). *R*_f = 0.10 (Only EtOAc); mp: 143.5–145.0 °C; ¹H NMR (400 MHz, CDCl₃) δ 8.87–8.88 (m, ArH), 8.64–8.66 (m, ArH), 8.04–8.08 (m, 2 ArH), 7.95–7.98 (m, ArH), 7.84 (d, *J* = 15.8 Hz, trans H), 7.66 (d, *J* = 15.7 Hz, trans H), 7.37–7.40 (m, ArH), 7.06–7.09 (m, 2 ArH), 4.82 (s, OCH₂), 3.13 (s, NCH₃), 3.02 (s, NCH₃); ¹³C NMR (100 MHz, CDCl₃) δ 188.0, 167.0, 162.0, 151.0, 149.9, 140.3, 134.5, 131.4, 130.8, 123.8, 123.7, 114.7, 100.9, 67.2, 36.5, 35.7; HRMS (M + H)⁺ (ESI⁺) 311.1383 [M + H]⁺ (calcd for C₁₈H₁₈N₂O₃H⁺ 311.1390).

4.1.23. (*E*)-*N,N*-Dimethyl-2-(4-(3-(pyridin-4-yl)acryloyl)phenoxy)acetamide (**14e**)

Using Method A, **13** (0.20 g, 0.90 mmol), 4-pyridinecarboxaldehyde (0.26 mL, 2.70 mmol) and LiOH·H₂O (0.05 g, 1.10 mmol) gave **14e** as a light yellow solid (0.10 g, 35%). *R*_f = 0.05 (Only EtOAc); mp: 146.0–147.5 °C; ¹H NMR (400 MHz, DMSO-*d*₆) δ 8.67 (d, *J* = 5.8 Hz, 2 ArH), 8.14–8.18 (m, 2 ArH, trans H), 7.84 (d, *J* = 5.8 Hz, 2 ArH), 7.65 (d, *J* = 15.6 Hz, trans H), 7.08 (d, *J* = 8.8 Hz, 2 ArH), 4.99 (s, OCH₂), 3.02 (s, NCH₃), 2.86 (s, NCH₃); ¹³C NMR (100 MHz, DMSO-*d*₆) δ 187.7, 167.0, 163.0, 150.8, 142.4, 140.7, 131.4, 130.6, 126.9, 122.9, 115.3, 66.2, 36.0, 35.4; HRMS (M + H)⁺ (ESI⁺) 311.1382 [M + H]⁺ (calcd for C₁₈H₁₈N₂O₃H⁺

311.1390).

4.1.24. (E)-1-(4-(2-Morpholino-2-oxoethoxy)phenyl)-3-(2-(trifluoromethyl)phenyl)prop-2-en-1-one (17a)

Using Method A, **16** (0.50 g, 1.90 mmol), 2-(trifluoromethyl)benzaldehyde (0.99 g, 5.7 mmol) and LiOH·H₂O (0.10 g, 2.28 mmol) gave **17a** as a light yellow solid (0.32 g, 40%). *R_f* = 0.55 (Only EtOAc); mp: 90.0–91.0 °C; ¹H NMR (400 MHz, CDCl₃) δ 8.11–8.15 (m, trans **H**), 8.03–8.06 (m, 2 Ar**H**), 7.84 (d, *J* = 7.7 Hz, Ar**H**), 7.75 (d, *J* = 7.8 Hz, Ar**H**), 7.63 (t, *J* = 7.52 Hz, Ar**H**), 7.52 (t, *J* = 7.68 Hz, Ar**H**), 7.42 (d, *J* = 15.6 Hz, trans **H**), 7.06–7.08 (m, 2 Ar**H**), 4.82 (s, OCH₂), 3.61–3.71 (m, 8 morpholine **H**); ¹³C NMR (75 MHz, CDCl₃) δ 188.5, 165.9, 161.6, 139.7 (d, *J* = 1.88 Hz), 134.2, 132.1, 131.6, 131.1, 129.6, 129.2 (q, *J* = 30.3 Hz), 128.0, 126.4, 126.3 (q, *J* = 5.5 Hz), 124.0 (q, *J*_{C-F} = 272.4 Hz), 114.6, 67.5, 66.8, 66.7, 45.9, 42.5; HRMS (M + H)⁺ (ESI⁺) 420.1415 [M + H]⁺ (calcd for C₂₂H₂₀F₃NO₄H⁺ 420.1417).

4.1.25. (E)-3-(2-Methoxyphenyl)-1-(4-(2-morpholino-2-oxoethoxy)phenyl)prop-2-en-1-one (17b)

Using Method A, **16** (0.30 g, 1.14 mmol), 2-methoxybenzaldehyde (0.31 g, 2.28 mmol) and LiOH·H₂O (0.06 g, 1.37 mmol) gave **17b** as a light yellow solid (0.18 g, 41%). *R_f* = 0.55 (Only EtOAc); mp: 114.5–115.5 °C; ¹H NMR (400 MHz, CDCl₃) δ 8.11 (d, *J* = 15.8 Hz, trans **H**), 8.03–8.07 (m, 2 Ar**H**), 7.62–7.66 (m, Ar**H**, trans **H**), 7.37–7.41 (m, Ar**H**), 6.95–7.07 (m, 4 Ar**H**), 4.80 (s, OCH₂), 3.94 (s, OCH₃), 3.62–3.71 (m, 8 morpholine **H**); ¹³C NMR (75 MHz, CDCl₃) δ 189.3, 166.0, 161.2, 158.8, 139.9, 132.5, 131.6, 130.9, 129.3, 124.1, 122.6, 120.8,

114.4, 111.3, 67.5, 66.8, 66.7, 55.6, 45.9, 42.5; HRMS (M + H)⁺ (ESI⁺) 382.1647 [M + H]⁺ (calcd for C₂₂H₂₃NO₅H⁺ 382.1649).

4.1.26. (E)-1-(4-(2-Morpholino-2-oxoethoxy)phenyl)-3-(pyridin-2-yl)prop-2-en-1-one (17c)

Using Method A, **16** (0.20 g 0.76 mmol), 2-pyridine carboxaldehyde (0.22 mL, 2.28 mmol) and LiOH·H₂O (0.04 g, 0.91 mmol) gave **17c** as a light yellow solid (0.16 g, 58%). *R_f* = 0.20 (Only EtOAc); mp: : 177.0–179.0 °C; ¹H NMR (400 MHz, DMSO-*d*₆) δ 8.70 (d, *J* = 3.9 Hz, ArH), 8.10–8.18 (m, 2 ArH, trans H), 7.91 (s, 2 ArH), 7.65 (d, *J* = 15.3 Hz, trans H), 7.43–7.44 (m, ArH), 7.02 (d, *J* = 8.3 Hz, 2 ArH), 5.02 (s, OCH₂), 3.59–3.64 (m, 8 morpholine H); ¹³C NMR (100 MHz, DMSO-*d*₆) δ 188.1, 166.0, 162.7, 162.4, 153.4, 153.4, 150.5, 142.8, 137.6, 131.2, 131.0, 125.6, 125.2, 125.1, 115.3, 66.5, 66.2, 45.1, 42.1; HRMS (M + H)⁺ (ESI⁺) 353.1493 [M + H]⁺ (calcd for C₂₀H₂₀F₃N₂O₄H⁺ 353.1496).

4.1.27. (E)-1-(4-(2-(4-Methylpiperazin-1-yl)-2-oxoethoxy)phenyl)-3-(2-(trifluoromethyl)phenyl)prop-2-en-1-one hydrochloride (20a)

19a (0.05 g, 0.12 mmol) was treated with HCl (4.0 M in dioxane) (0.043 mL, 0.17 mmol) to give a salt form **20a** as a light yellow solid (0.04 g, 71%). mp: 98.0–100.0 °C; ¹H NMR (400 MHz, DMSO-*d*₆) δ 11.05 (s, N⁺H), 8.33 (d, *J* = 7.8 Hz, ArH), 8.18 (d, *J* = 8.76 Hz, 2 ArH), 8.04 (d, *J* = 15.3 Hz, trans H), 7.95 (d, *J* = 15.3 Hz, trans H), 7.78–7.86 (m, 2 ArH), 7.67 (t, *J* = 7.6 Hz, ArH), 7.11 (d, *J* = 8.72 Hz, ArH), 5.08 (s, OCH₃), 4.39 (br s, piperazine H), 4.04 (br s, piperazine H), 3.34–3.43 (2 br s, 3 piperazine H), 2.96–3.11 (2 br s, 3 piperazine H),

2.78 (s, NCH₃); ¹³C NMR (75 MHz, DMSO-*d*₆) δ 187.5, 166.1, 162.7, 137.6, 133.4, 132.6, 131.4, 131.1, 130.9, 130.8, 130.6, 129.3, 128.8, 126.8, 126.6, 126.0, 115.3, 66.1, 52.4, 42.5, 41.5, 38.7, remained aromatic peak was overlapped with other signals; HRMS (M + H)⁺ (ESI⁺) 433.1731 [M + H]⁺ (calcd for C₂₃H₂₄ClF₃N₂O₃H⁺ 433.1734).

4.1.28. (E)-3-(2-Methoxyphenyl)-1-(4-(2-(4-methylpiperazin-1-yl)-2-oxoethoxy)phenyl) prop-2-en-1-one hydrochloride (20b)

19b (0.10 g, 0.25 mmol) was treated with HCl (4.0 M in dioxane) (0.095 mL, 0.38 mmol) to give a salt form **20b** as a light ivory solid (0.10 g, 94%). mp: 225.0–227.0 °C; ¹H NMR (400 MHz, DMSO-*d*₆) δ 10.75 (s, N⁺H), 8.11 (d, *J* = 8.4 Hz, 2 ArH), 7.96–8.04 (m, ArH, trans H), 7.87 (d, *J* = 15.6 Hz, trans H), 7.45 (t, *J* = 7.8 Hz, ArH), 7.02–7.13 (m, 4 ArH), 5.06 (s, OCH₃), 4.40 (br s, piperazine H), 4.03 (br s, piperazine H), 3.90 (s, OCH₃), 3.35–3.44 (2 br s, 3 piperazine H), 2.97–3.09 (2 br s, 3 piperazine H), 2.79 (s, NCH₃); ¹³C NMR (75 MHz, DMSO-*d*₆) δ 188.1, 166.2, 162.4, 158.7, 138.3, 132.6, 131.6, 131.1, 128.9, 123.6, 122.4, 121.2, 115.2, 112.3, 66.1, 56.2, 52.6, 52.4, 42.5, 41.5, 35.9; HRMS (M + H)⁺ (ESI⁺) 395.1963 [M + H]⁺ (calcd for C₂₃H₂₇ClN₂O₄H⁺ 395.1965).

4.1.29. (E)-3-(2-Fluorophenyl)-1-(4-(2-(4-methylpiperazin-1-yl)-2-oxoethoxy)phenyl) prop-2-en-1-one hydrochloride (20c)

19c (0.10 g, 0.26 mmol) was treated with HCl (4.0 M in dioxane) (0.098 mL, 0.39 mmol) to give a salt form **20c** as a white solid (0.11 g, 98%). mp: 243.5–244.0 °C; ¹H NMR (400 MHz, DMSO-*d*₆) δ 10.99 (s, HCl), 8.11–8.15 (m, 3 ArH), 7.99 (d, *J* = 15.7 Hz, trans H), 7.81 (d, *J*

= 15.7 Hz, trans **H**), 7.50–7.55 (m, Ar**H**), 7.31–7.35 (m, 2 Ar**H**), 7.10 (d, $J = 8.7$ Hz, 2 Ar **H**), 5.07 (s, OCH₃), 4.38 (br s, piperazine **H**), 4.02 (br s, piperazine **H**), 3.40–3.56 (2br s, 3 piperazine **H**), 2.99–3.11 (2br s, 3 piperazine **H**), 2.77 (s, NCH₃); ¹³C NMR (100 MHz, DMSO-*d*₆) δ 187.7, 166.2, 162.6, 161.3 (d, $J_{C-F} = 253.1$), 134.8 (d, $J_{C-F} = 4.1$ Hz), 133.0 (d, $J_{C-F} = 8.77$ Hz), 131.3, 131.0, 129.6, 125.4 (d, $J_{C-F} = 3.3$ Hz), 124.7 (d, $J_{C-F} = 4.1$ Hz), 112.9 (d, $J_{C-F} = 11.1$ Hz), 116.5 (d, $J_{C-F} = 21.6$ Hz), 115.3, 66.0, 52.5, 52.4, 42.5, 41.5, 38.7; HRMS (M + H)⁺ (ESI⁺) 383.1763 [M + H]⁺ (calcd for C₂₂H₂₄ClFN₂O₃H⁺ 383.1765).

4.1.30. (E)-3-(2-Chlorophenyl)-1-(4-(2-(4-methylpiperazin-1-yl)-2-oxoethoxy)phenyl)prop-2-en-1-one hydrochloride (20d)

19d (0.10 g, 0.25 mmol) was treated with HCl (4.0 M in dioxane) (0.094 mL, 0.38 mmol) to give a salt form **20d** as a white solid (0.09 g, 85%). mp: 237.0–239.0 °C; ¹H NMR (400 MHz, DMSO-*d*₆) δ 10.75, (s, HCl), 8.16–8.23 (m, 3 Ar**H**), 7.97–8.05 (m, 2 trans **H**), 7.57–7.59 (m, Ar **H**), 7.44–7.51 (m, 2 Ar**H**), 7.11 (d, $J = 8.5$ Hz, 2 Ar **H**), 5.07 (s, OCH₂), 4.39 (br s, piperazine **H**), 4.03 (br s, piperazine **H**), 3.43 (br s, 3 piperazine **H**), 2.97–3.09 (2 br s, 3 piperazine **H**), 2.78 (s, NCH₃); ¹³C NMR (75 MHz, DMSO-*d*₆) δ 187.7, 161.2, 162.7, 138.3, 134.7, 132.9, 132.3, 131.3, 131.0, 130.4, 129.0, 128.1, 125.4, 115.5, 66.1, 52.4, 52.3, 42.5, 41.5, 38.7; HRMS (M + H)⁺ (ESI⁺) 399.1466 [M + H]⁺ (calcd for C₂₂H₂₄Cl₂N₂O₃H⁺ 399.1470).

4.1.31. (E)-1-(4-(2-(4-Methylpiperazin-1-yl)-2-oxoethoxy)phenyl)-3-phenylprop-2-en-1-one hydrochloride (20e)

19e (0.10 g, 0.27 mmol) was treated with HCl (4.0 M in dioxane) (0.10 mL, 0.41 mmol) to give a salt form **20e** as a white solid (0.11 g, 95%). mp: 244.5–245.0 °C; ¹H NMR (400 MHz, DMSO-*d*₆) δ 10.80 (s, **HCl**), 8.15 (d, *J* = 8.8 Hz, 2 Ar**H**), 7.88–7.96 (m, Ar**H**, trans **H**), 7.71 (d, *J* = 15.5 Hz, trans **H**), 7.46–7.47 (m, 3 Ar**H**), 7.09 (d, *J* = 8.8 Hz, 2 Ar**H**), 5.07 (s, O**CH**₂), 4.41 (br s, piperazine **H**), 4.03 (br s, piperazine **H**), 3.43 (br s, 3 piperazine **H**), 2.98–3.09 (2br s, 3 piperazine **H**), 2.79 (s, N**CH**₃); ¹³C NMR (100 MHz, DMSO-*d*₆) δ 187.9, 166.1, 162.6, 143.7, 137.6, 135.3, 132.3, 130.9, 129.4, 129.3, 112.6, 115.2, 66.0, 52.5, 52.4, 42.5, 41.5, 38.7; HRMS (*M* + *H*)⁺ (ESI⁺) 365.1857 [*M* + *H*]⁺ (calcd for C₂₂H₂₅ClN₂O₃H⁺ 365.1860).

4.2. Cell culture

BV-2 microglial cells were cultured in RPMI 1640 (Biowest, Nuaille, France) supplemented with 10% fetal bovine serum (Biowest), 2.05 mM L-glutamine (Gibco, Thermo Fisher Scientific, Waltham, MA, USA), and 100 U/mL penicillin-streptomycin (Gibco) at 37 °C in a 5% CO₂ humidified incubator. For the Keap1-Nrf2 nuclear translocation assay, the PathHunter[®] U2OS Keap1-NRF2 nuclear translocation cell line (93-0821C3, DiscoverX, Fremont, CA, USA) was cultured in AssayComplete[™] cell culture medium (92-3103G, DiscoverX) at 37 °C in a 5% CO₂ humidified incubator.

4.3. Keap1-Nrf2 nuclear translocation assay

The Nrf2 nuclear translocation activity of each synthesized compound was evaluated using the PathHunter[®] eXpress Keap1-NRF2 nuclear translocation assay kit (93-0821E3CP0L,

DiscoverX) according to the manufacturer's instruction. The PathHunter[®] U2OS nuclear translocation cells were engineered to co-express enzyme donor-tagged NRF2 and nuclear-localized enzyme acceptor. Activation of Nrf2 induces complementation of the enzyme fragments through nuclear translocation of Nrf2, resulting in the formation of functional β -galactosidase, the activity of which was detected by chemiluminescence. The engineered U2OS cells were seeded in 96-well white plates and treated with various concentrations of the test compound for 6 h at room temperature (20–23 °C). After incubating the cells for 1 h with detection reagent in the dark, the chemiluminescent signals were detected at all wavelengths using a microplate reader (SpectraMax[®] i3, Molecular Device, San Jose, CA, USA). The EC₅₀ value of each compound was calculated as the mean \pm SEM in triplicate from the concentration- response curve using SigmaPlot software version 13.0.

4.4. Cytotoxicity assay

The cytotoxicity of compound **20a** was evaluated using the WST-based Ez-Cytox cell viability assay kit (DoGenBio, Seoul, South Korea). Cell viability was determined based on the amount of orange-colored formazan dye produced from WST by the mitochondrial dehydrogenases present only in living cells. BV-2 microglial cells were seeded in 96-well plates and incubated with various concentrations of compound **20a** for 24 h at 37 °C. After 1 h of treatment with Ez-Cytox reagent, cell viability was quantified by measuring the absorbance at 450 nm using a microplate reader (SpectraMax[®] i3, Molecular Device).

4.5. Quantitative real-time PCR analysis

Total RNA was isolated from BV-2 microglial cells using TRIzol[®] reagent (Invitrogen, Thermo Fisher Scientific) according to the manufacturer's instructions. Complementary DNA (cDNA) was synthesized from 500 ng total RNA using iScript[™] gDNA Clear cDNA Synthesis Kit (Bio-Rad, Hercules, CA, USA). Real-time PCR was performed with CFX Connect[™] Real-Time PCR Detection System (Bio-Rad) using iQ[™] SYBR[®] Green Supermix (Bio-Rad). Gene expression was normalized relative to *Hprt*. The following primer sequences were used: *Ho-1*, 5'-CAGCCACACAGCACTATG-3' (Forward) and 5'-GCAATC TTCTTCAGGACCT-3' (Reverse); *Gclm*, 5'-GGAGCTTCGGGACTGTATCC-3' (Forward) and 5'-TCGGGATTTATCTTC TCCAATGC-3' (Reverse).

4.6. SDS-PAGE and immunoblotting

BV-2 microglial cells were washed with ice-cold phosphate-buffered saline (PBS) and lysed on ice for 40 min using RIPA lysis buffer (Sigma-Aldrich, St. Louis, MO, USA) containing protease inhibitor cocktail (Roche Diagnostics Corp., Indianapolis, IN, USA). After centrifugation at $15800 \times g$ for 20 min, the supernatant was transferred to a new tube to obtain whole cell lysate. Nuclear fractionation was performed according to a protocol previously described by Woo *et al.* [39] After protein quantification using the Pierce[®] BCA Protein Assay Kit (Thermo Fisher Scientific), equal amounts (10 μ g) of protein were separated on SDS-polyacrylamide minigels and transferred onto a polyvinylidene fluoride (PVDF) membrane (Millipore, Burlington, MA, USA). The membranes were blocked with 5% skim milk in TBST (10 mM Tris-HCl, pH 7.5, 150 mM NaCl, and 0.1% Tween[®] 20) for 1 h at room temperature and probed overnight with primary antibodies specific for Nrf2 (Cell Signaling Technology, 1:500), HO-1 (Enzo Life Sciences, 1:1000), GCLM (Santa Cruz

Biotechnology, 1:1000), SOD1 (Abcam, 1:2000), iNOS (Abcam, 1:500), Lamin B1 (Bioworld Technology, 1:3000), or β -Actin (Santa Cruz Biotechnology, 1:2000) at 4 °C. Blots were then incubated with anti-rabbit or anti-mouse horseradish peroxidase (HRP)-conjugated secondary antibodies (GeneTex, 1:10,000) for 1 h at room temperature. The protein bands were developed using Amersham enhanced chemiluminescence detection reagent (GE Healthcare, Chicago, IL, USA) and visualized using the Amersham Imager 600 (GE Healthcare). Relative protein intensities were analyzed by ImageJ software (NIH) and normalized to Lamin B1 or β -Actin.

4.7. Griess assay

The concentration of nitric oxide (NO) in the cell culture medium was determined by measuring nitrite (NO_2^-), one of the two major stable breakdown products of NO, using the Griess assay. BV-2 microglial cells were pre-treated with various concentrations of compound **20a** for 6 h and stimulated with 1 $\mu\text{g}/\text{mL}$ LPS for 24 h. Then, 50 μL of each culture medium was mixed with 50 μL sulfanilamide solution (1% sulfanilamide in 5% phosphoric acid) and incubated for 5 min at room temperature in the dark. Fifty microliters of NED solution (0.1% N-1-naphthylethylenediamine dihydrochloride in water) was added and incubated for 5 min at room temperature in the dark. Nitrite levels were determined by measuring the absorbance at 540 nm using a microplate reader (SpectraMax[®] i3, Molecular Device) and comparing with a nitrite standard curve.

4.8. Enzyme-linked immunosorbent assay (ELISA) for proinflammatory cytokines

BV-2 microglial cells were seeded in 12-well plates and pre-incubated with various concentrations of compound **20a** for 3 h. After stimulation with 0.2 $\mu\text{g}/\text{mL}$ LPS for 24 h, TNF- α and IL-6 in the cell culture medium were measured using ELISA kits (eBioscience, San Diego, CA, USA) according to the manufacturer's instructions.

4.9. Intracellular ROS assay

Intracellular ROS production was measured using the cell-permeable probe, DCFH-DA (Sigma-Aldrich). In cells, DCFH-DA is deacetylated by cellular esterases and rapidly oxidized to highly fluorescent 2',7'-dichlorofluorescein (DCF) by ROS; the fluorescence intensity within the cells is proportional to the intracellular ROS levels. BV-2 microglial cells were seeded in 96-well black plates and treated with various concentrations of compound **20a** for 24 h at 37 °C. Then, the cells were incubated with 20 μM DCFH-DA for 40 min and 200 μM H_2O_2 was added to the culture medium for an additional 20 min at 37 °C in the dark. The fluorescence intensity was measured by a microplate reader (SpectraMax[®]*i3*, Molecular Device) with an excitation wavelength of 480 nm and an emission wavelength of 530 nm.

4.10. Imaging of intracellular ROS accumulation

Intracellular ROS was localized using DCFH-DA. BV-2 microglial cells were treated with various concentrations of compound **20a** for 24 h at 37 °C. The cells were incubated with 40 μM DCFH-DA for 40 min and 300 μM H_2O_2 was added to the culture medium for an additional 20 min at 37 °C in the dark. After washing with PBS, fluorescent images were captured with a CELENA[®] S Digital Imaging System (Logos Biosystems, South Korea).

4.11. SOD activity assay

SOD activity was measured using a SOD assay kit (Dojindo, Kumamoto, Japan) according to the manufacturer's instructions. This SOD assay utilizes WST-1 (2-(4-iodophenyl)-3-(4-nitrophenyl)-5-(2,4-disulfophenyl)-2H-tetrazolium, monosodium salt), which produces a formazan dye upon reduction with superoxide anion, and this WST-1 reduction is inhibited by SOD. Therefore, the inhibitory activity of SOD was determined by measuring the absorbance of the WST-1 formazan. BV-2 microglial cells (1.0×10^6 cells) were treated with compound **20a** for 6 h, followed by 400 μ M H_2O_2 for 18 h. The cells were harvested and washed twice with PBS. After centrifugation at $2340 \times g$ for 3 min, the cells were resuspended in 200 μ L ice-cold PBS and sonicated on an ice bath (60 W with 1 s intervals for 30 s). Then, the cell lysate was centrifuged at $15800 \times g$ for 20 min at 4 °C and the supernatant was analyzed immediately. For *in vivo* SOD activity measurements, hippocampus tissue was collected from vehicle- and scopolamine-treated mice (2 mg/kg, *i.p.*) with or without oral administration of compound **20a** (30 mg/kg/day for 5 days). Immediately following dissection, the tissue was homogenized in ten volumes (w/v) sucrose buffer (0.25 M sucrose, 10 mM Tris, 1 mM EDTA, pH 7.4). The hippocampus homogenate was centrifuged at $15800 \times g$ for 40 min at 4 °C and the supernatant was used for analysis. SOD activity was calculated by the IC_{50} values determined from the SOD inhibition curve using SigmaPlot software version 13.0, and is expressed as units (U) per milligram of protein, wherein 1 U of SOD is defined as the amount of the SOD in sample solution that inhibits the reduction of WST-1 with superoxide anion by 50%.

4.12. Animals and treatment

Male C57BL/6N mice (age, 10 weeks; weight, 25–27 g) were purchased from Orient Bio (Seoul, South Korea) and housed in a temperature- and humidity-controlled environment (22 ± 1 °C, 12 h light-dark cycle) with free access to food and water. All mice were handled according to the directives of the Animal Care and Use Committee of the Institutional Animal Care and Use Committee of KIST (Seoul, South Korea). For behavioral experiments, the mice were randomly assigned to three treatment groups: (1) vehicle (saline), (2) scopolamine (1 mg/kg or 2 mg/kg), and (3) scopolamine (1 mg/kg or 2 mg/kg) with compound **20a** (30 mg/kg/day). Compound **20a** was dissolved in saline and administered by oral gavage (*p.o.*) once daily for 5 days. Scopolamine hydrobromide (Sigma-Aldrich) was dissolved in saline and injected intraperitoneally (*i.p.*) 30 min before the Y-maze test and the acquisition trial of the passive avoidance test.

4.13. Y-maze test

The Y-maze apparatus consisted of three identical arms made of black plastic at a 120° angle from each other (41 × 7 × 15 cm). All mice were handled daily for 7 days prior to testing. Each mouse was placed at the end of one arm facing the center of the maze and allowed to freely explore for 10 min. The arm entries were recorded manually and it was considered an entry when all four paws of the mouse were within the arm. An alternation was defined as consecutive entries into each of the three different arms. The percentage of spontaneous alternations was calculated based on the following equation: $\text{alternation (\%)} = \text{number of alternations} / (\text{total arm entries} - 2) \times 100$.

4.14. Passive avoidance test

The step-through passive avoidance test was conducted in a two-compartment chamber with one illuminated and one dark compartment separated by a guillotine door (GEMINI™ Avoidance System, San Diego Instruments, San Diego, CA, USA). All mice were handled daily for 7 days prior to the trial. On the acquisition trial day, each mouse was placed individually in the illuminated compartment and allowed to explore for 30 s. After 30 s, the guillotine door was raised and the mouse was allowed to freely enter the dark compartment. Immediately after the mouse entered the dark compartment, the door was closed and an electric foot shock (0.3 mA, 1 s duration) was delivered through the grid floor after 3 s. Then, after 30 s, the mouse was returned to the home cage. Twenty-four hours after the acquisition trial, the mouse was placed again in the illuminated compartment for the retention trial and allowed to explore for 15 s; the guillotine door was then raised. The step-through latency to enter the dark compartment after the door was opened was measured up to a maximum of 540 s in both the acquisition and retention trials.

4.15. Statistical analyses

The data are presented as mean \pm SEM. The data were analyzed using unpaired two-tailed Student's *t*-test, one-way ANOVA with *Tukey's* multiple comparisons test, or one-way ANOVA with *Dunnett's* multiple comparisons test by GraphPad Prism 7 software. The statistical significance level is displayed as asterisks ($*p < 0.05$, $**p < 0.01$, $***p < 0.001$; n.s. not significant).

Abbreviations

AD, Alzheimer's disease; ARE, antioxidant response element; DCFH-DA, 2', 7'-Dichlorodihydrofluorescein diacetate; DMF, dimethyl fumarate; GCL, glutamate-cysteine ligase; GCLM, glutamate-cysteine ligase regulatory subunit; HO-1, heme oxygenase-1; H₂O₂, hydrogen peroxide; IL-6, interleukin 6; iNOS, inducible nitric oxide synthase; Keap1, kelch-like ECH-associated protein 1; LPS, lipopolysaccharide; NO, nitric oxide; Nrf2, nuclear factor E2-related factor 2; ROS, reactive oxygen species; Scop, scopolamine; SOD, superoxide dismutase ; TNF- α , tumor necrosis factor α

Declaration of interest

The authors declare no conflict of interest.

Acknowledgments

This study was supported by the National Research Council of Science & Technology (NST) grant by the Korea government (MSIP) (grant numbers CRC-15-04-KIST), the National Research Foundation of Korea (grant numbers NRF-2018M3A9C8016849).

References

- [1] R. Jakob-Roetne, H. Jacobsen, Alzheimer's disease: from pathology to therapeutic approaches, *Angew. Chem., Int. Ed.* 48 (2009) 3030-3059.
- [2] C.L. Masters, R. Bateman, K. Blennow, C.C. Rowe, R.A. Sperling, J.L. Cummings, Alzheimer's disease, *Nat. Rev. Dis. Primers* 1 (2015) 15056.
- [3] T. Wyss-Coray, Inflammation in Alzheimer disease: driving force, bystander or beneficial response?, *Nat. Med.* 12 (2006) 1005-1015.
- [4] H.L. Weiner, D. Frenkel, Immunology and immunotherapy of Alzheimer's disease, *Nat. Rev. Immunol.* 6 (2006) 404-416.
- [5] E. Solito, M. Sastre, Microglia function in Alzheimer's disease, *Front. Pharmacol.* 3 (2012) 14.
- [6] K. Taguchi, H. Motohashi, M. Yamamoto, Molecular mechanisms of the Keap1-Nrf2 pathway in stress response and cancer evolution, *Genes Cells* 16 (2011) 123-140.
- [7] T.W. Kensler, N. Wakabayashi, S. Biswal, Cell survival responses to environmental stresses via the Keap1-Nrf2-ARE pathway, *Annu. Rev. Pharmacol. Toxicol.* 47 (2007) 89-116.
- [8] M.P. Soares, M.P. Seldon, I.P. Gregoire, T. Vassilevskaia, P.O. Berberat, J. Yu, T.-Y. Tsui, F.H. Bach, Heme oxygenase-1 modulates the expression of adhesion molecules associated with endothelial cell activation, *J. Immunol.* 172 (2004) 3553-3563.
- [9] A. Banning, P.R. Brigelius-Flohé, NF- κ B, Nrf2, and HO-1 interplay in redox-regulated VCAM-1 expression, *Antioxid. Redox Signal.* 7 (2005) 889-899.
- [10] K. Itoh, M. Mochizuki, Y. Ishii, T. Ishii, T. Shibata, Y. Kawamoto, V. Kelly, K. Sekizawa, K. Uchida, M. Yamamoto, Transcription factor Nrf2 regulates inflammation by mediating the effect of 15-deoxy-12,14-prostaglandin J2, *Mol. Cell. Biol.* 24 (2003) 36-45.
- [11] H. Motohashi, M. Yamamoto, Nrf2-Keap1 defines a physiologically important stress

response mechanism, *Trends. Mol. Med.* 10 (2004) 549-557.

[12] E.H. Kobayashi, T. Suzuki, R. Funayama, T. Nagashima, M. Hayashi, H. Sekine, N. Tanaka, T. Moriguchi, H. Motohashi, K. Nakayama, M. Yamamoto, Nrf2 suppresses macrophage inflammatory response by blocking proinflammatory cytokine transcription, *Nat. Commun.* 7 (2016) 11624.

[13] S.M. Ahmed, L. Luo, A. Namani, X.J. Wang, X. Tang, Nrf2 signaling pathway: pivotal roles in inflammation, *Biochim. Biophys. Acta, Mol. Basis Dis.* 1863 (2017) 585-597.

[14] R.K. Thimmulappa, H. Lee, T. Rangasamy, S.P. Reddy, M. Yamamoto, T.W. Kensler, S. Biswal, Nrf2 is a critical regulator of the innate immune response and survival during experimental sepsis, *J. Clin. Invest.* 116 (2016) 984-995.

[15] W. Li, T.O. Khor, C. Xu, G. Shen, W.-S. Jeong, S. Yu, A.-N. Kong, Activation of Nrf2-antioxidant signaling attenuates NF κ B-inflammatory response and elicits apoptosis, *Biochem. Pharmacol.* 76 (2008) 1485-1489.

[16] Joanna D. Wardyn, Amy H. Ponsford, Christopher M. Sanderson, Dissecting molecular cross-talk between Nrf2 and NF- κ B response pathways, *Biochem. Soc. Trans.* 43 (2015) 621-626.

[17] X. Liu, X. Zhang, Y. Ding, W. Zhou, L. Tao, P. Lu, Y. Wang, R. Hu, Nuclear factor E2-related factor-2 negatively regulates NLRP3 inflammasome activity by inhibiting reactive oxygen species-induced NLRP3 priming, *Antioxid. Redox Signal.* 26 (2017) 28-43.

[18] X. Liu, W. Zhou, X. Zhang, P. Lu, Q. Du, L. Tao, Y. Ding, Y. Wang, R. Hu, Dimethyl fumarate ameliorates dextran sulfate sodium-induced murine experimental colitis by activating Nrf2 and suppressing NLRP3 inflammasome activation, *Biochem. Pharmacol.* 112 (2016) 37-49.

[19] M.J. Calkins, D.A. Johnson, J.A. Townsend, M.R. Vargas, J.A. Dowell, T.P. Williamson,

A.D. Kraft, J.M. Lee, J. Li, J.A. Johnson, The Nrf2/ARE pathway as a potential therapeutic target in neurodegenerative disease, *Antioxid. Redox Signal.* 11 (2009) 497-508.

[20] T. Suzuki, H. Motohashi, M. Yamamoto, Toward clinical application of the Keap1-Nrf2 pathway, *Trends Pharmacol. Sci.* 34 (2013) 340-346.

[21] C.P. Ramsey, C.A. Glass, M.B. Montgomery, K.A. Lindl, G.P. Ritson, L.A. Chia, R.L. Hamilton, C.T. Chu, K.L. Jordan-Sciutto, Expression of Nrf2 in neurodegenerative diseases, *J. Neuropathol. Exp. Neurol.* 66 (2007) 75-85.

[22] K. Kanninen, T.M. Malm, H.K. Jyrkkanen, G. Goldsteins, V. Keksa-Goldsteine, H. Tanila, M. Yamamoto, S. Ylä-Herttuala, A.L. Levonen, J. Koistinaho, Nuclear factor erythroid 2-related factor 2 protects against beta amyloid, *Mol. Cell. Neurosci.* 39 (2008) 302-313.

[23] L. Yu, S. Wang, X. Chen, H. Yang, X. Li, Y. Xu, X. Zhu, Orientin alleviates cognitive deficits and oxidative stress in A β 1-42-induced mouse model of Alzheimer's disease, *Life Sci.* 121 (2015) 104-109.

[24] K. Kanninen, R. Heikkinen, T. Malm, T. Rolova, S. Kuhmonen, H. Leinonen, S. Ylä-Herttuala, H. Tanila, A.-L. Levonen, M. Koistinaho, J. Koistinaho, Intrahippocampal injection of a lentiviral vector expressing Nrf2 improves spatial learning in a mouse model of Alzheimer's disease, *Proc. Natl. Acad. Sci. U. S. A.* 106 (2009) 16505-16510.

[25] J.A. Lee, H. J. Son, J.W. Choi, J. Kim, S.H. Han, N. Shin, J.H. Kim, S.J. Kim, J.Y. Heo, D.J. Kim, K.D. Park, O. Hwang, Activation of the Nrf2 signaling pathway and neuroprotection of nigral dopaminergic neurons by a novel synthetic compound KMS99220, *Neurochem. Int.* 112 (2018) 96-107.

[26] V. Kumar, S. Kumar, M. Hassan, H. Wu, R.K. Thimmulappa, A. Kumar, S.K. Sharma, V.S. Parmar, S. Biswal, S.V. Malhotra, Novel chalcone derivatives as potent Nrf2 activators

in mice and human lung epithelial cells, *J. Med. Chem.* 54 (2011) 4147-4159.

[27] J. Wu, J. Li, Y. Cai, Y. Pan, F. Ye, Y. Zhang, Y. Zhao, S. Yang, X. Li, G. Liang, Evaluation and discovery of novel synthetic chalcone derivatives as anti-inflammatory agents, *J. Med. Chem.* 54 (2011) 8110-8123.

[28] V.R. Yadav, S. Prasad, B. Sung, B.B. Aggarwal, The role of chalcones in suppression of NF- κ B-mediated inflammation and cancer, *Int. Immunopharmacol.* 11 (2011) 295-309.

[29] L.Cong, X. Dong, Y. Wang, Y. Deng, B. Li, R. Dai, On the role of synthesized hydroxylated chalcones as dual functional amyloid- β aggregation and ferroptosis inhibitors for potential treatment of Alzheimer's disease, *Eur. J. Med. Chem.* 166 (2019) 11-21.

[30] J.C. Espinoza-Hicks, K.F. Chacon-Vargas, J.L. Hernandez-Rivera, B. Noguera-Torres, J. Tanariz, L.E. Sanchez-Torres, A. Camacho-Davila, Novel prenyloxy chalcones as potential leishmanicidal and trypanocidal agents: Design, synthesis and evaluation, *Eur. J. Med. Chem.* 167 (2019) 402-413.

[31] F. Xu, W. Li, W. Shuai, L. Yang, Y. Bi, C. Ma, H. Yao, S. Xu, Z. Zhu, J. Xu, Design, synthesis and biological evaluation of pyridine-chalcone derivatives as novel microtubule-destabilizing agents, *Eur. J. Med. Chem.* 173 (2019) 1-14.

[32] L.F. Castano, V. Cuartas, A. Bernal, A. Insuasty, J. Guzman, O. Vidal, V. Rubio, G. Puerto, P. Lukac, V. Vimberg, G. Balkova-Novtona, L. Vannucci, J. Janata, J. Quiroga, R. Abonia, M. Nogueras, J. Cobo, B. Insuasty, New chalcone-sulfonamide hybrids exhibiting anticancer and antituberculosis activity, *Eur. J. Med. Chem.* 176 (2019) 50-60

[33] A. Rampa, S. Montanari, L. Pruccoli, M. Bartolini, F. Falchi, A. Feoli, A. Cavalli, F. Belluti, S. Gobbi, A. Tarozzi, A. Bisi, Chalcone-based carbamates for Alzheimer's disease treatment, *Future Med. Chem.* (2017) 749-764.

[34] X. Zhang, K.P. Rakesh, S.N.A. Bukhari, M. Balakrishna, H.M. Manukumar, H.-L. Qin,

Multi-targetable chalcone analogs to treat deadly Alzheimer's disease: Current view and upcoming advice, *Bioorg. Chem.* 80 (2018) 86-93.

[35] Y.J. Jang, J. Kim, J. Shim, C.Y. Kim, J.H. Jang, K.W. Lee, H.J. Lee, Decaffeinated coffee prevents scopolamine-induced memory impairment in rats, *Behav. Brain Res.* 245 (2013) 113-119.

[36] A. Ahmad, K. Ramasamy, S.M. Jaafar, A.B. Majeed, V. Mani, Total isoflavones from soybean and tempeh reversed scopolamine-induced amnesia, improved cholinergic activities and reduced neuroinflammation in brain, *Food Chem. Toxicol.* 65 (2014) 120-128.

[37] I. Klinkenberg, A. Blokland, The validity of scopolamine as a pharmacological model for cognitive impairment: a review of animal behavioral studies, *Neurosci. Biobehav. Rev.* 34 (2010) 1307-1350.

[38] S.H. Kwon, H.K. Lee, J.A. Kim, S.I. Hong, H.C. Kim, T.H. Jo, Y.I. Park, C.K. Lee, Y.B. Kim, S.Y. Lee, C.G. Jang, Neuroprotective effects of chlorogenic acid on scopolamine-induced amnesia via anti-acetylcholinesterase and anti-oxidative activities in mice, *Eur. J. Pharmacol.* 649 (2010) 210-217.

[39] N.E. Kouemou, G.S. Taiwe, F.C.O. Moto, S. Pale, G.T. Ngoupaye, J.S.K. Njapdounke, G.C.N. Nkantchoua, D.B. Pahaye, E.N. Bum, Nootropic and neuroprotective effects of *dichrocephala integrifolia* on scopolamine mouse model of Alzheimer's disease, *Front. Pharmacol.* 8 (2017) 847.

[40] J.W. Choi, S. Kim, J.-H. Park, H.J. Kim, S.J. Shin, J.W. Kim, S.Y. Woo, C. Lee, S.M. Han, J. Lee, A.N. Pae, G. Han, K.D. Park, Optimization of vinyl sulfone derivatives as potent Nuclear factor erythroid 2-related factor 2 (Nrf2) activators for Parkinson's disease therapy, *J. Med. Chem.* 62 (2019) 811-830.

[41] J.-H. Park, J.W. Choi, E.J. Ju, A.N. Pae, K.D. Park, Antioxidant and anti-inflammatory

activities of a natural compound, shizukahenriol, through Nrf2 activation, *Molecules* 20 (2015) 15989-16003.

[42] S.Y. Woo, J.H. Kim, M.K. Moon, S.-H. Han, S.K. Yeon, J.W. Choi, B.K. Jang, H.J. Song, Y.G. Kang, J.W. Kim, J. Lee, D.J. Kim, O. Hwang, K.D. Park, Discovery of vinyl sulfones as a novel class of neuroprotective agents toward Parkinson's disease therapy, *J. Med. Chem.* 57 (2014) 1473-1487.

[43] S.H. Lee, D.H. Sohn, X.Y. Jin, S.W. Kim, S.C. Choi, G.S. Seo, 2',4',6'-Tris(methoxymethoxy) chalcone protects against trinitrobenzene sulfonic acid-induced colitis and blocks tumor necrosis factor- α -induced intestinal epithelial inflammation via heme oxygenase 1-dependent and independent pathways, *Biochem. Pharmacol.* 74 (2007) 870-880.

[44] I. Bellezza, A. Tucci, F. Galli, S. Grottelli, A.L. Mierla, F. Pilolli, A. Minelli, Inhibition of NF- κ B nuclear translocation via HO-1 activation underlies α -tocopheryl succinate toxicity, *J. Nutr. Biochem.* 23 (2012) 1583-1591.

[45] T. Jiang, F. Tian, H. Zheng, S.A. Whitman, Y. Lin, Z. Zhang, N. Zhang, D.D. Zhang, Nrf2 suppresses lupus nephritis through inhibition of oxidative injury and the NF- κ B-mediated inflammatory response, *Kidney Int.* 85 (2014) 333-343.

[46] U. Bayani, V.S. Ajay, Z. Paolo, R.T. Mahajan, Oxidative stress and neurodegenerative diseases: a review of upstream and downstream antioxidant therapeutic options, *Curr. Neuropharmacol.* 7 (2009) 65-74.

[47] M.A. Ansari, S.W. Scheff, Oxidative stress in the progression of Alzheimer disease in the frontal cortex, *J. Neuropathol. Exp. Neurol.* 69 (2010) 155-167.

[48] Y. Ihara, T. Hayabara, K. Sasaki, Y. Fujisawa, R. Kawada, T. Yamamoto, Y. Nakashima, S. Yoshimune, M. Kawai, M. Kibata, S. Kuroda, Free radicals and superoxide dismutase in blood of patients with Alzheimer's disease and vascular dementia, *J. Neurol. Sci.* 153 (1997)

76-81.

[49] H. Vural, H. Demirin, Y. Kara, I. Eren, N. Delibas, Alterations of plasma magnesium, copper, zinc, iron and selenium concentrations and some related erythrocyte antioxidant enzyme activities in patients with Alzheimer's disease, *J. Trace Elem. Med. Bio.* 24 (2010) 169-173.

[50] S.I. Mota, R.O. Costa, I.L. Ferreira, I. Santana, G.L. Caldeira, C. Padovano, A.C. Fonseca, I. Baldeiras, C. Cunha, L. Letra, C.R. Oliveira, C.M.F. Pereira, A.C. Rego, Oxidative stress involving changes in Nrf2 and ER stress in early stages of Alzheimer's disease, *Biochim. Biophys. Acta, Mol. Basis Dis.* 1852 (2015) 1428-1441.

[51] A.-V. Noemí, A. Giulia, P. Chiara, M. Carmen, C. Fernando, M. Manuel, M. Mariagrazia, C.-G. David, F.-S. María Teresa, N. Antonello, M. Maurizio, U. Daniela, Comparison of extracellular and intracellular blood compartments highlights redox alterations in Alzheimer's and mild cognitive impairment patients, *Curr. Alzheimer Res.* 14 (2017) 112-122.

[52] C. Chong, L. Xiao-Hong, Z. Sai, T. Yue, W. Yan-Min, S. Hong-Tao, 7,8-dihydroxyflavone ameliorates scopolamine-induced Alzheimer-like pathologic dysfunction, *Rejuven. Res.* 17 (2014) 249-254.

[53] M.-T. Hsieh, C.-L. Hsieh, L.-W. Lin, C.-R. Wu, G.S. Huang, Differential gene expression of scopolamine-treated rat hippocampus-application of cDNA microarray technology, *Life Sci.* 73 (2003) 1007-1016.

[54] S.W. Bihagi, A.P. Singh, M. Tiwari, Supplementation of *Convolvulus pluricaulis* attenuates scopolamine-induced increased tau and Amyloid precursor protein (A β PP) expression in rat brain, *Indian J. Pharmacol.* 44 (2012) 593-598.

[55] A.T. Dinkova-Kostova, M.A. Massiah, R.E. Bozak, R.J. Hicks, P. Talalay, Potency of Michael reaction acceptors as inducers of enzymes that protect against carcinogenesis

depends on their reactivity with sulfhydryl groups, *Proc. Natl. Acad. Sci. U. S. A.* 98 (2001) 3404-3409.

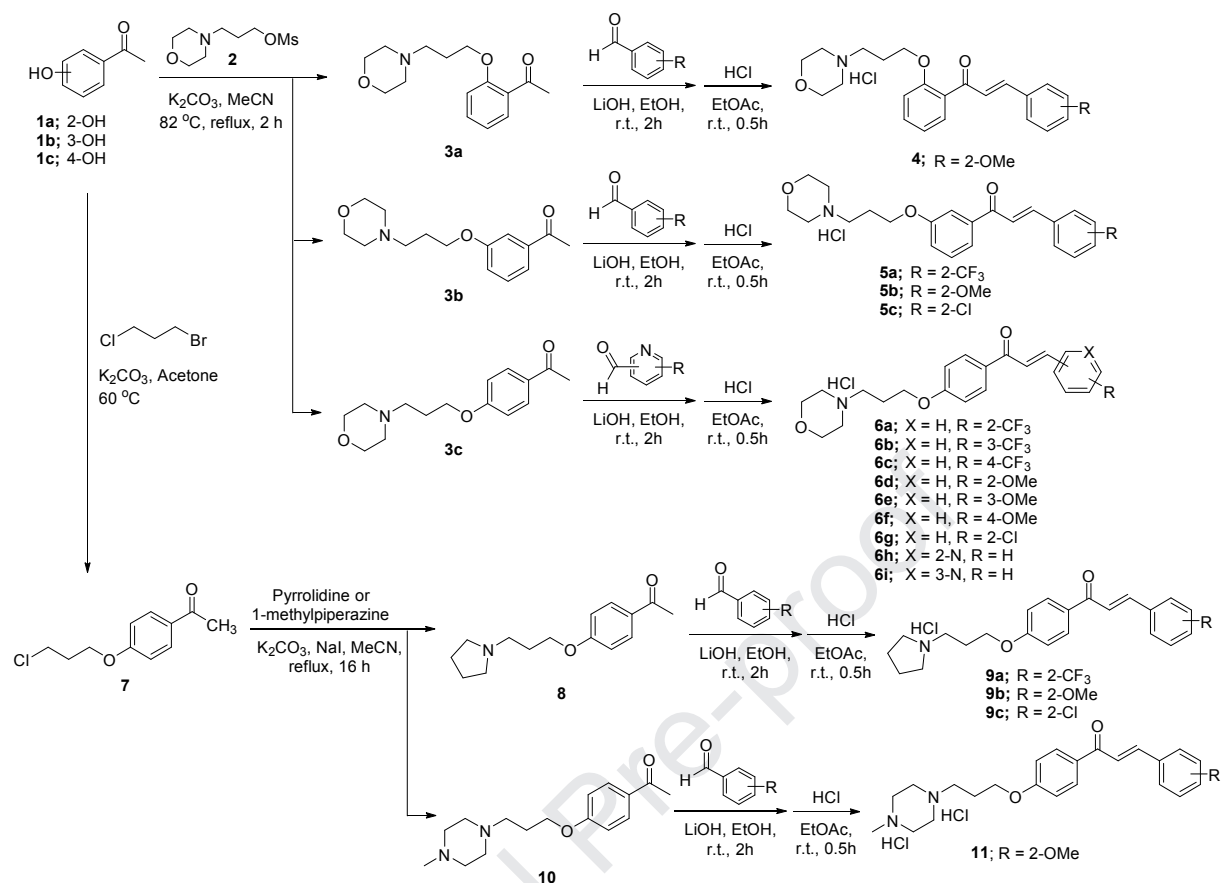
[56] R. Kaur, S. Mehan, D. Khanna, K. Kalra, Ameliorative treatment with ellagic acid in scopolamine induced Alzheimer's type memory and cognitive dysfunctions in rats, *Austin J. Clin. Neurol.* 2 (2015) 1053.

[57] C. Guo, J. Shen, Z. Meng, X. Yang, F. Li, Neuroprotective effects of polygalacic acid on scopolamine-induced memory deficits in mice, *Phytomedicine* 23 (2016) 149-155.

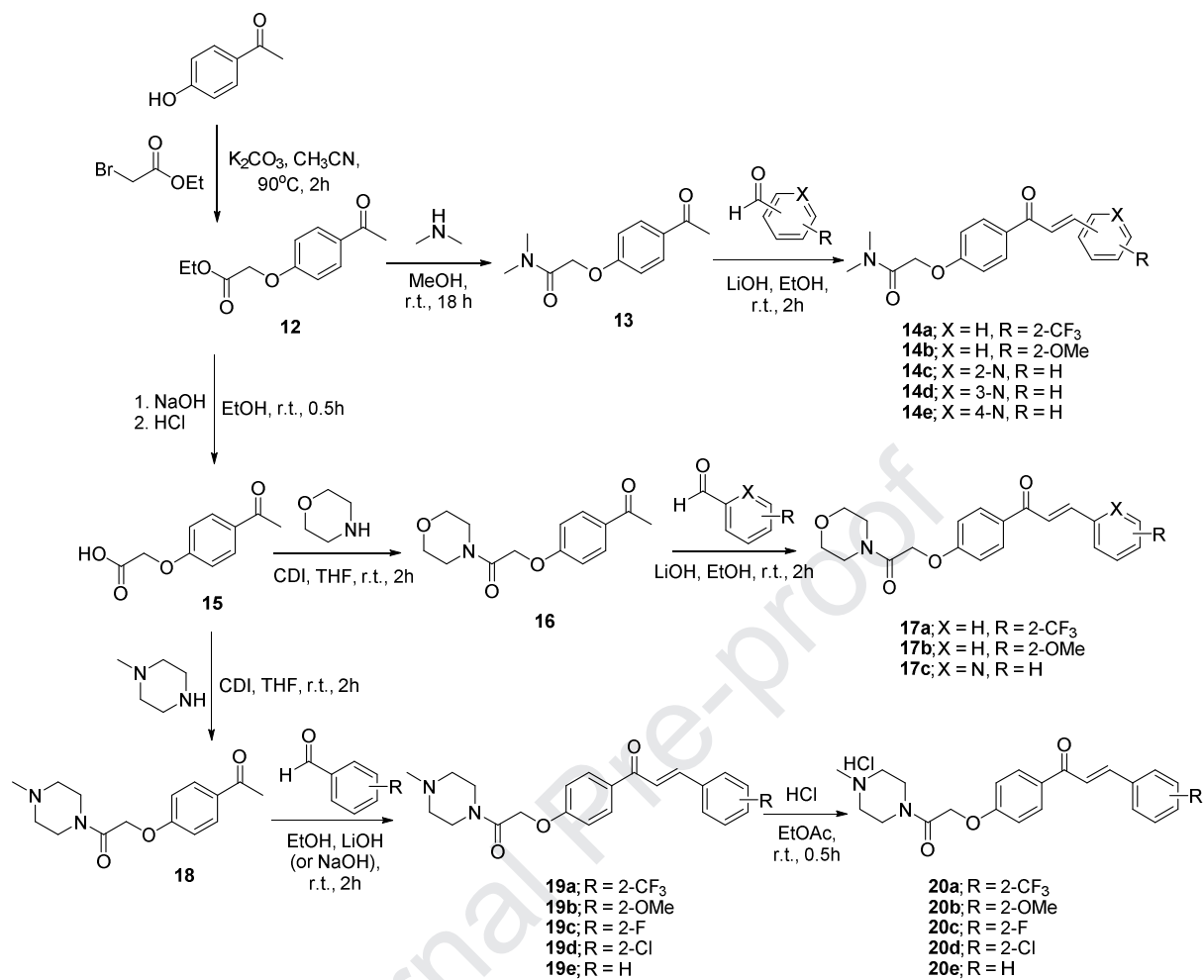
Journal Pre-proof

(EC₅₀) values shown. The modified U2OS cells were seeded in 96-well plate and treated with various concentrations of the compound in triplicate for 6 h. ^bPositive controls; SFN: sulforaphane, a well-known potent activator of Nrf2. ^cPositive controls; DMF: dimethyl fumarate (Tecfidera™), a well-known potent activator of Nrf2 approved by FDA for the treatment of Multiple sclerosis. ^dEC₅₀ value of the compound could not be determined due to cytotoxicity.

Journal Pre-proof



Scheme 1. Synthetic scheme of compounds 4, 5, 6, 9 and 11



Scheme 2. Synthetic scheme of compounds 14, 17, and 20

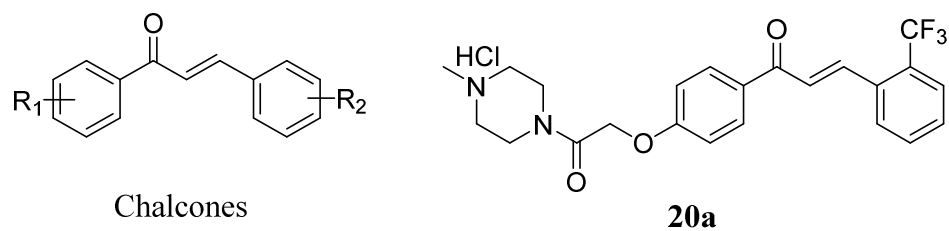


Figure 1. Chemical structures of representative chalcone and compound 20a

Journal Pre-proof

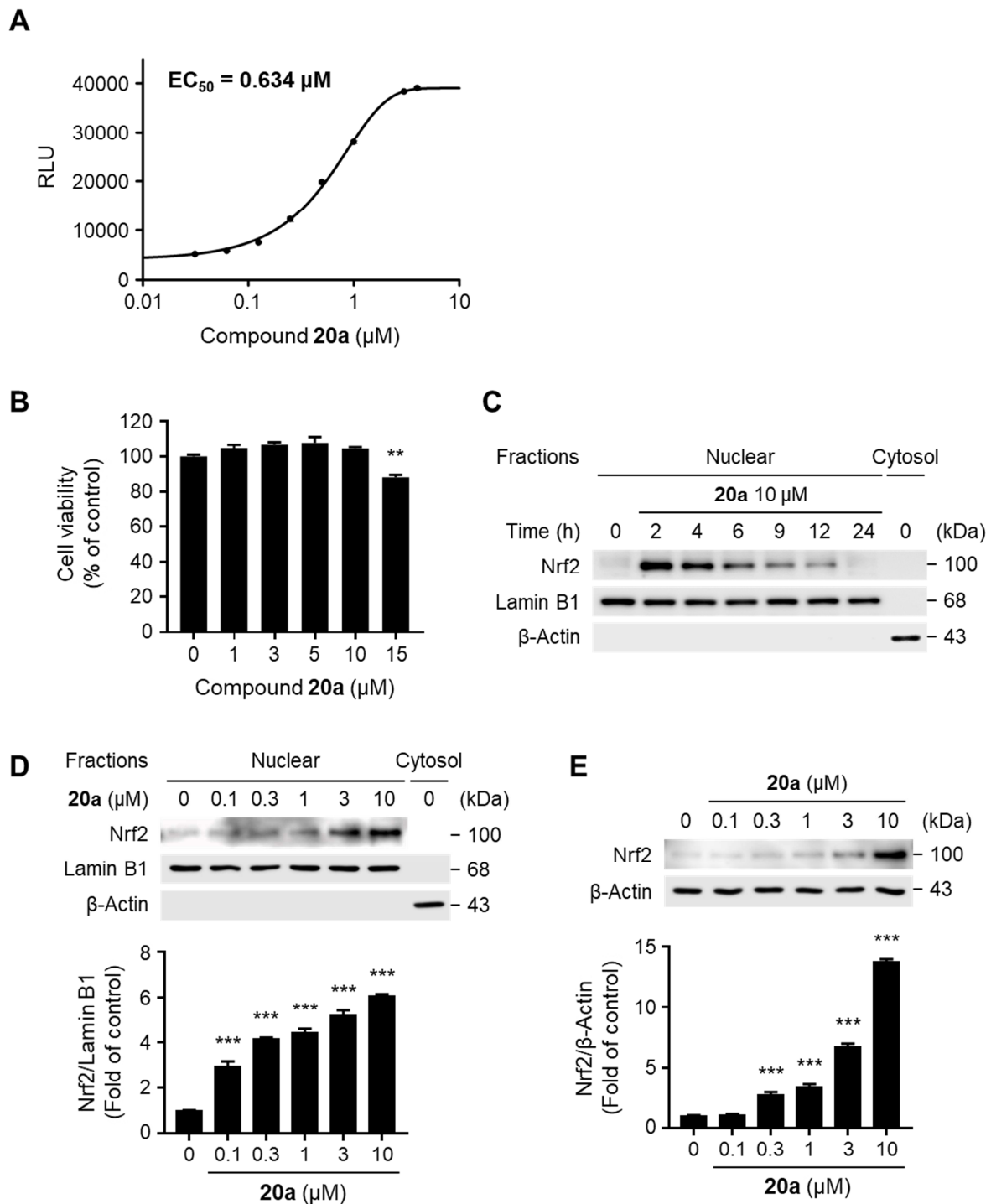


Figure 2. Compound 20a induces nuclear translocation and cellular accumulation of Nrf2. (A) Concentration-response curve of compound 20a for Nrf2 activation in Keap1-Nrf2 nuclear translocation assay (n=3 assays). Nrf2 activating efficacy was measured in relative light units (RLU) evoked by nuclear translocation of Nrf2 in modified U2OS cells. (B) Cell viability at 24 h after treatment of 20a in BV-2 microglial cells. (C) Time-dependent effects of compound 20a on nuclear Nrf2 level in BV-2 microglial cells. (D, E) Western blot analyses of Nrf2 protein levels in nuclear extracts (D) or cell lysates (E) of BV-2 microglial

cells after 6 h treatment with **20a**. Data are presented as means \pm SEM. $**p < 0.01$, $***p < 0.001$, compared with untreated control (One-way ANOVA with *Dunnett's* test).

Journal Pre-proof

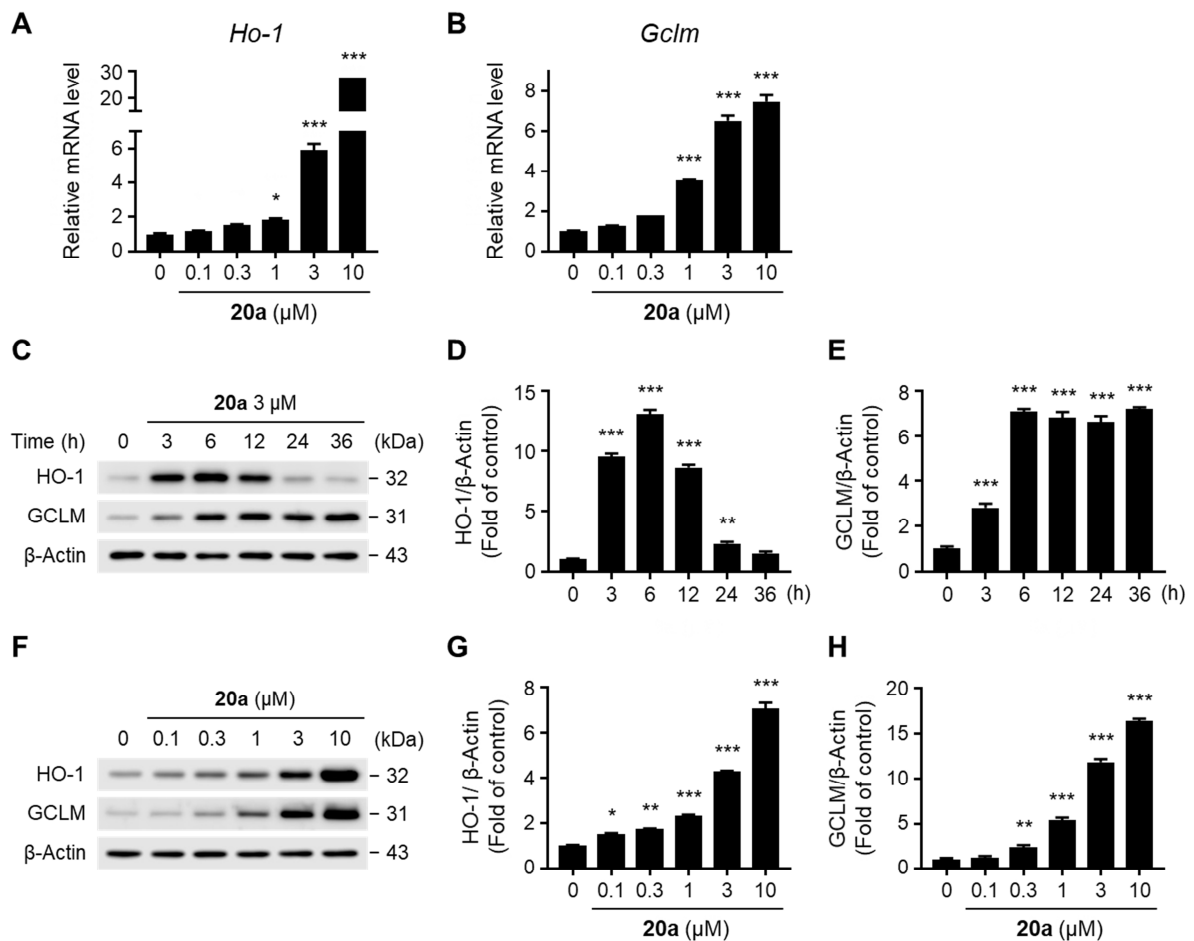


Figure 3. Compound 20a induces gene expression of Nrf2-dependent antioxidant enzymes. (A, B) Relative mRNA expression of *Ho-1* (A) and *Gclm* (B) in BV-2 microglial cells after 8 h treatment with various concentrations of **20a**. *Hprt* mRNA levels were used to normalize the expression of *Ho-1* and *Gclm*. (C) Time-dependent effects of compound **20a** on protein expression of HO-1 and GCLM in BV-2 microglial cells. (D, E) Densitometric analyses of HO-1 (D) and GCLM (E) in the western blots of (C). Data were normalized to the internal control β -Actin. (F) Western blot analyses of HO-1 and GCLM in BV-2 microglial cells after 12 h treatment with various concentrations of **20a**. (G, H) Densitometric analyses of HO-1 (G) and GCLM (H) in the western blots of (F). Data are presented as means \pm SEM. * $p < 0.05$, ** $p < 0.01$, *** $p < 0.001$, compared with untreated control (One-way ANOVA with *Dunnett's* test).

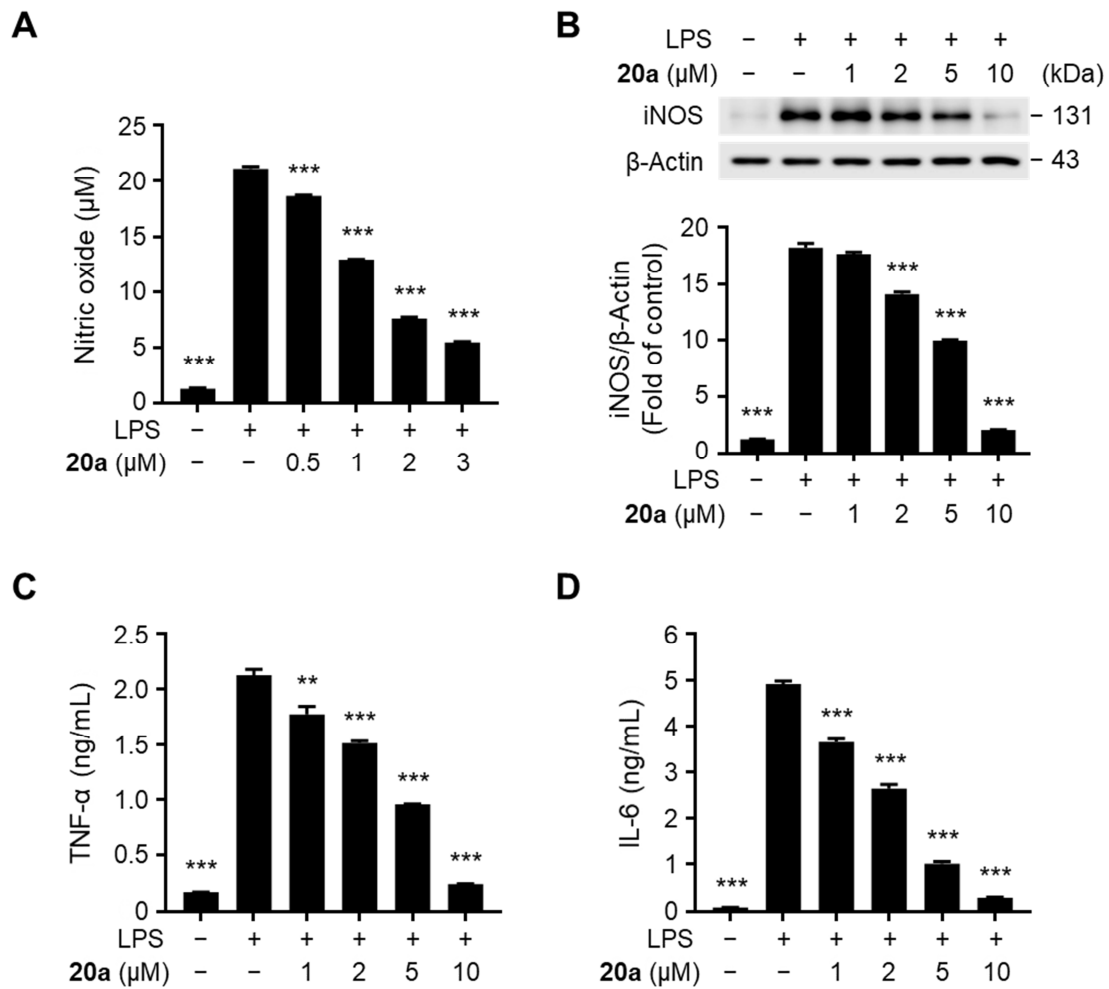


Figure 4. Compound 20a attenuates LPS-induced inflammation in BV-2 microglial cells. (A) NO levels in culture medium of LPS-stimulated BV-2 microglial cells pretreated with compound **20a** for 6 h. (B) Western blot analysis of iNOS in LPS-stimulated BV-2 cells after 3 h pretreatment with **20a**. (C, D) The concentration of TNF- α (C) or IL-6 (D) secreted into culture medium from LPS-stimulated BV-2 cells, as measured by ELISA. Data are presented as means \pm SEM. ** $p < 0.01$, *** $p < 0.001$, compared with LPS-treated control (One-way ANOVA with *Dunnnett's* test).

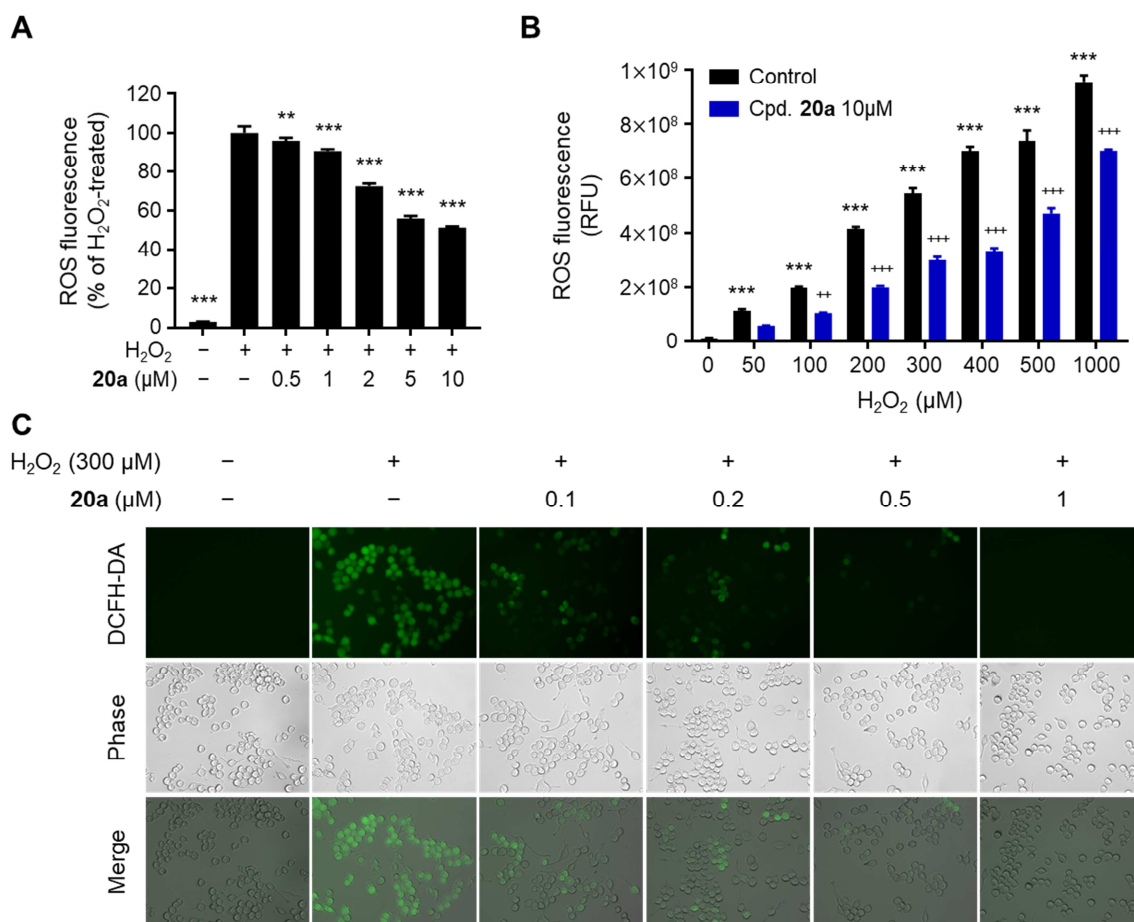


Figure 5. Compound 20a suppresses H₂O₂-induced oxidative stress in BV-2 microglial cells. (A, B) Effects of compound 20a on H₂O₂-induced ROS production. Intracellular ROS levels measured using DCFH-DA. (A) BV-2 microglial cells were pretreated with the indicated concentrations of 20a for 24 h and exposed to 200 μM H₂O₂ for 20 min. (B) BV-2 microglial cells were pretreated with 10 μM compound 20a for 24 h and exposed to the indicated concentrations of H₂O₂ for 20 min. (C) Representative fluorescence microscopy images of DCFH-DA-stained BV-2 cells. Data are presented as means ± SEM. ***p* < 0.01, ****p* < 0.001, compared with H₂O₂-treated control (A) or untreated control (B). ++*p* < 0.01, +++*p* < 0.001, compared with each equal concentration of H₂O₂-treated control (B) (One-way ANOVA with *Dunnnett's* test (A) or One-way ANOVA with *Tukey's* test (B)).

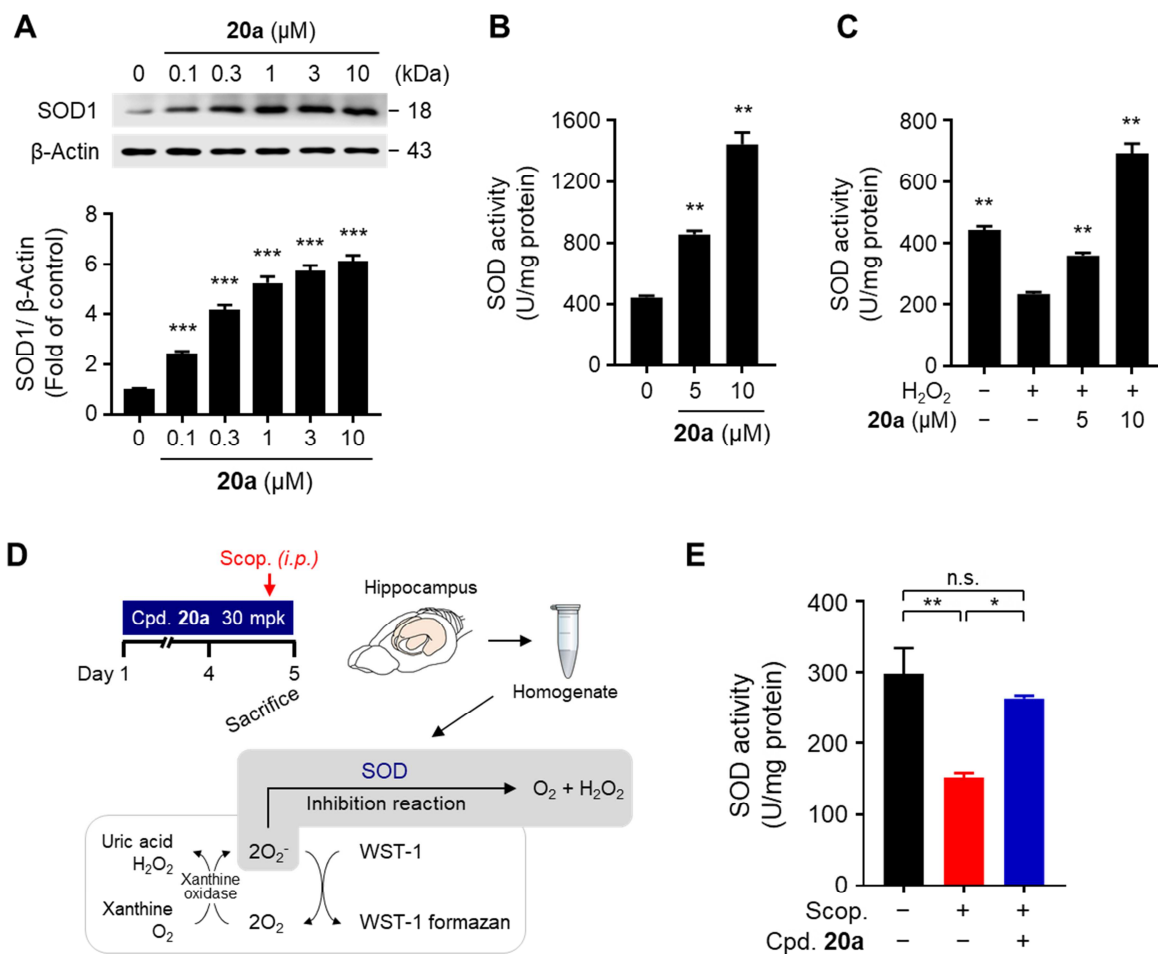


Figure 6. Compound 20a increases gene expression and activity of SOD *in vitro* and *in vivo*. (A) Western blot analyses of SOD1 in BV-2 microglial cells after 6 h treatment with various concentrations of **20a**. (B, C) Effects of compound **20a** on SOD activity of BV-2 microglial cells in normal conditions (B) or exposed to 400 μM H₂O₂ for 18 h (C). (D) Reaction diagram of the enzyme activity assay of SOD in the hippocampus. (E) Effect of compound **20a** (30 mg/kg/day for 5 days, *p.o.*) on SOD activity in brain hippocampus of vehicle- and scopolamine-treated mice (2 mg/kg, *i.p.*). Data are presented as means ± SEM. **p* < 0.05, ***p* < 0.01, ****p* < 0.001, compared with untreated control (A, B) or H₂O₂-treated control (C); n.s. not significant (One-way ANOVA with *Dunnnett's* test (A), unpaired Student's *t*-test (B, C) or One-way ANOVA with *Tukey's* test (E)). Scop, scopolamine.

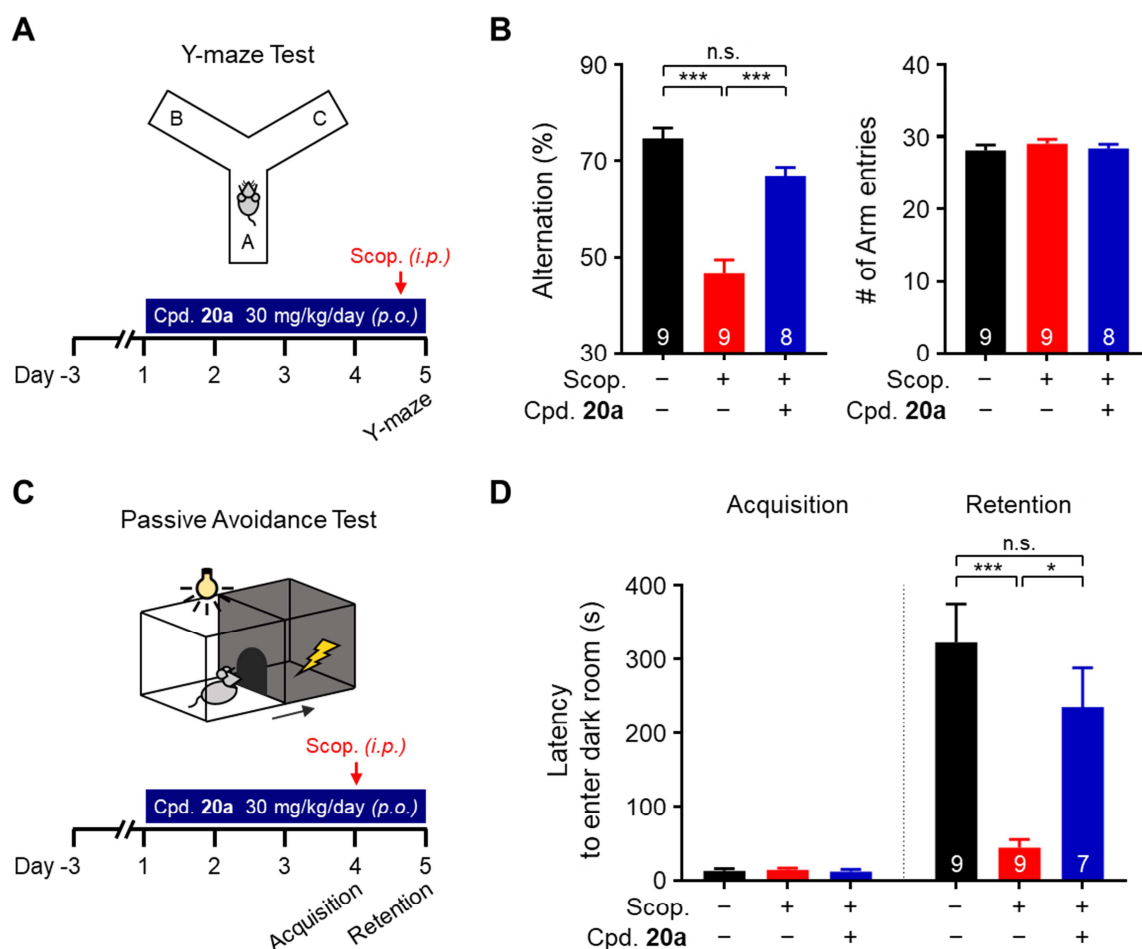


Figure 7. Compound 20a restores learning and memory in the scopolamine-induced amnesia model. (A, C) Schematic diagram (top) and experimental protocol (bottom) for Y-maze test (A) or passive avoidance test (C) from vehicle- and scopolamine-treated mice (2 mg/kg (A) or 1 mg/kg (C), *i.p.*) with or without oral administration of compound 20a (30 mg/kg/day for 5 days). (B) Percentage of spontaneous alternations (left) and total number of arm entries (right) in Y-maze test. (D) Latency to enter dark room in passive avoidance test. Data are presented as means \pm SEM. * $p < 0.05$, *** $p < 0.001$; n.s. not significant (One-way ANOVA with *Tukey's* test). Scop, scopolamine. Numbers within the bars in (B) and (D) refers to the number of mice analyzed.

Graphical Abstract

